Check for updates

Journal of Vegetation Science

RESEARCH ARTICLE OPEN ACCESS

Turning Mediterranean Farmlands Into Priority Habitats: Natural Expansion of Juniper Woodlands After Agricultural Abandonment

Laura Bentley[1,2] | Alicia Forner[3,4] | Sacha Khoury[1] | Fernando Valladares[3,5] | David A. Coomes[1] | Irene Martín-Forés[3,6,7]

[1]Department of Plant Sciences and Conservation Research Institute, University of Cambridge, Cambridge, UK | [2]UK Centre for Ecology and Hydrology, Environment Centre Wales, Bangor, UK | [3]Laboratorio Internacional de Cambio Global (LINCGlobal), Departamento Biogeografía y Cambio Global, Museo Nacional de Ciencias Naturales, MNCN-CSIC, Madrid, Spain | [4]Faculty of Education, Internacional University of La Rioja (UNIR), La Rioja, Spain | [5]Departamento de Biología y Geología, Escuela Superior de Ciencias Experimentales y Tecnológicas, Universidad Rey Juan Carlos, Móstoles, Spain | [6]School of Biological Sciences, Adelaide University, Adelaide, South Australia, Australia | [7]College of Science and Engineering, Flinders University, Bedford Park, South Australia, Australia

Correspondence: Irene Martín-Forés (irene.martin@adelaide.edu.au) | Alicia Forner (alicia.forner@unir.net)

Received: 21 November 2025 | **Revised:** 28 March 2026 | **Accepted:** 10 April 2026

Coordinating Editor: Eric Lamb

Keywords: biomass | forest | *Juniperus thurifera* | landscape ecology | land-use change | natural colonisation | plant–plant interactions | remote sensing | structure-from-motion

ABSTRACT

Aims: Natural woodland expansion into former agricultural land contributes to conservation and global reforestation goals. However, tree colonisation and woodland persistence depend on interactions among vegetation, land-use history and suitable microclimatic conditions. Understanding these drivers is essential for anticipating woodland expansion outcomes over large spatial and temporal scales.

Methods: We combined airborne photogrammetry with field measurements to assess the long-term success of *Juniperus thurifera* woodlands—a Natura 2000 priority habitat—across a 20-km^2 region of central Spain. A canopy height model, calibrated with field biomass data, was used to map juniper biomass, while time series land-cover maps estimated woodland age. This novel approach enabled evaluation of colonisation success using a space-for-time substitution along the expansion frontier.

Results: Over the past 34 years, land cover has changed markedly, with agricultural land declining by 75% and open woodland tripling. Juniper stands have expanded from steep slopes onto flatter terrain and into areas with lower irradiance. Increasing dwarf-shrub density within stands reduced juniper biomass by up to 25% in the oldest woodlands. Higher solar exposure promoted faster biomass accumulation through time but limited biomass in younger stands. Contrarily, new stands under lower insolation showed greater biomass for their age, suggesting positive land-use legacies where drought stress was reduced.

Conclusion: Overall, *J. thurifera* woodlands have expanded substantially over recent decades, yet growth constraints differ across the expansion front. With our innovative framework integrating high-resolution photogrammetry and field-based biomass models, our study underscores the interplay between local competition and abiotic factors in shaping woodland dynamics across space and time. This framework offers a valuable, scalable and transferable tool for monitoring and managing long-term

Laura Bentley and Alicia Forner equally contributed to this study.

David A. Coomes and Irene Martín-Forés are both senior authors of this manuscript and contributed similarly.

This is an open access article under the terms of the Creative Commons Attribution-NonCommercial License, which permits use, distribution and reproduction in any medium, provided the original work is properly cited and is not used for commercial purposes.

© 2026 The Author(s). *Journal of Vegetation Science* published by John Wiley & Sons Ltd on behalf of International Association for Vegetation Science.

ecosystem dynamics across larger spatial and temporal scales and informing habitat restoration and conservation planning under changing environmental conditions.

1 | Introduction

Following declines in agriculture on marginal lands in the 20th century, and subsequent rural exodus, Europe's forested area naturally increased by 9% (20.4 million ha) from 1990 to 2020, contributing to international commitments to forest and woodland expansion (Dave et al. 2018; International Union for Conservation of Nature 2011; United Nations General Assembly 2015; Frei et al. 2024). Woodland expansion onto abandoned agricultural land sequesters carbon and may restore ecosystem services including soil fertility, water infiltration, and biodiversity (Cunningham et al. 2015; Martín-Forés et al. 2020). Landscape-level assessments of the environmental conditions that enable natural woodland expansion are crucial for the success of international commitments over the coming decades (Lamb 2018; Malhi et al. 2020; Seddon et al. 2020). Natural woodland expansion is known to be influenced by many biotic and abiotic factors, based on many local-scale studies. It may be impeded by sub-optimal soil and microclimate conditions (Poyatos et al. 2003; Cramer et al. 2007; Oldén et al. 2016; Jung et al. 2018). For example, in Portugal, natural colonisation of holm oak was strongly affected by solar exposure, which modulated near-ground temperature and moisture availability (Príncipe et al. 2014). Prolonged farming alters soil properties, affecting the structure of grass and shrub communities, further impacting woodland regeneration through competition (Bobbink et al. 2010; Sato et al. 2016, 2019). However, herb and shrub layers can also protect young trees from extreme climates and facilitate their establishment (Castro et al. 2004; Douaihy et al. 2022; Granda et al. 2014; Smit et al. 2008). In other examples, forests expanding into old fields can benefit from land-use legacies such as higher soil nitrogen and microbial activity, leading to increased tree growth and adaptation to water limitation (Freschet et al. 2014; Alfaro-Sánchez et al. 2019; Acuña-Míguez et al. 2020; Guerrieri et al. 2021). Assessing the net impact of these interacting factors is challenging at the landscape scale, and to the best of our knowledge, no previous studies have attempted to scale up from local observations to broader scales, which is crucial though that is for evaluating the health and viability of new natural woodlands as sources of carbon sequestration (Vilà-Cabrera et al. 2017; Cook-Patton et al. 2020), particularly in the context of climate change (Matesanz and Valladares 2014; Gazol et al. 2018; Camarero et al. 2018; Astigarraga et al. 2020).

Among European countries undergoing natural forest regrowth, Spain has the highest rate of natural forest expansion (i.e., 155.6000 ha per year; Forest Europe 2020), particularly in the mountainous regions in the North and Southeast of the country (Rodríguez-García et al. 2011; Vayreda et al. 2016). Several species are currently expanding their cover in Southern Europe. These include *Fagus sylvatica* L. in northern Spain, *Juniperus thurifera* L. in central Spain, *Quercus ilex* L. in northeastern Spain and *Quercus robur* L. in southwestern France (Hampe et al. 2020; Martín-Forés et al. 2020; Biodiversa+ 2022). Of these species, expansion of Spanish juniper (*J. thurifera*) is particularly interesting, because it is recognised as a priority species for conservation and the open and monospecific woodlands typically formed by this species are a priority habitat (Davies et al. 2004). Spanish juniper was heavily exploited for timber and fodder prior to its declaration as priority habitat; but is now recovering following a reduction in the abundance of livestock (Gauquelin et al. 1999; Olano et al. 2008; Montesinos and Fabado 2015), allowing expansion into abandoned grazing land (Martín-Forés et al. 2022). However, in these human-modified habitats, Spanish juniper is likely to encounter new biotic and abiotic circumstances (García Morote et al. 2012; Gimeno, Escudero, et al. 2012; Pías et al. 2014; Villellas et al. 2020). Also, slow-growing juniper is at a competitive disadvantage against most co-occurring tree species, although its tolerance to fluctuating temperatures and water availability (including sub-zero temperatures and extreme drought) allows it to grow outside the range of most competitors (Rozas et al. 2008; DeSoto et al. 2010; Gimeno, Camarero, et al. 2012). Sexual dimorphism has also been observed in response to growth stressors for this species, with female growth being more sensitive to summer drought but outgrowing males in mesic conditions (Olano et al. 2015; DeSoto et al. 2016). Thus, a combination of factors affects the potential success for the expansion and regrowth of this priority habitat, and there are ongoing concerns that changing management and range shifts amongst competing species may impact recovery (DeSoto et al. 2010).

Remote sensing technologies provide an opportunity to understand natural colonisation processes at landscape scales and close the current knowledge gap (see Huang et al. 2009; Tian et al. 2023). In particular, the three-dimensional structure of the land and vegetation can be mapped at high resolution using structure-from-motion (SFM) techniques applied to airborne remote sensing data. Combining field-based measurements with these technological advances offers unique insights into colonisation processes at scales not possible with traditional methods (Chen et al. 2022). Previous studies have either used remote sensing to map land-use cover and woodland expansion (Allen et al. 2018; Levers et al. 2018; Príncipe et al. 2014) or allometry to compare properties of expanding forests and mature stands at small spatial scales (Ruiz-Peinado et al. 2011). However, these methods are rarely combined.

Here, we quantify juniper woodland expansion in central Spain and seek to understand the factors influencing expansion. To do this, we study juniper growth at landscape, stand and individual tree scales. At the landscape scale, satellite imagery spanning 34 years is used to evaluate land cover change. At a local scale, factors limiting woodland expansion are analysed using individual juniper tree data mapped over a 20-km^2 area from high-resolution airborne imagery, combined with field-based allometric measurements to generate biomass estimates. This approach allowed us to evaluate the interacting effects of multiple factors affecting the expansion of this slow-growing, conservation-priority species from both a historical and a landscape perspective. We expected that (i) juniper woodland has expanded over the last 34 years, primarily into flatter areas made available by agricultural abandonment; (ii) that growth would be slower on sites exposed to greater insolation, as a consequence of greater water stress; and (iii) that juniper experiencing greater intra- and interspecific competition would exhibit slower growth.

16541103, 2026, 3, Downloaded from https://onlinelibrary.wiley.com/doi/10.1111/jvs.70142 by ALICIA FORNER - Spanish Cochrane National Provision (Ministerio de Sanidad) , Wiley Online Library on [04/05/2026]. See the Terms and Conditions (https://onlinelibrary.wiley.com/terms-and-conditions) on Wiley Online Library for rules of use; OA articles are governed by the applicable Creative Commons License

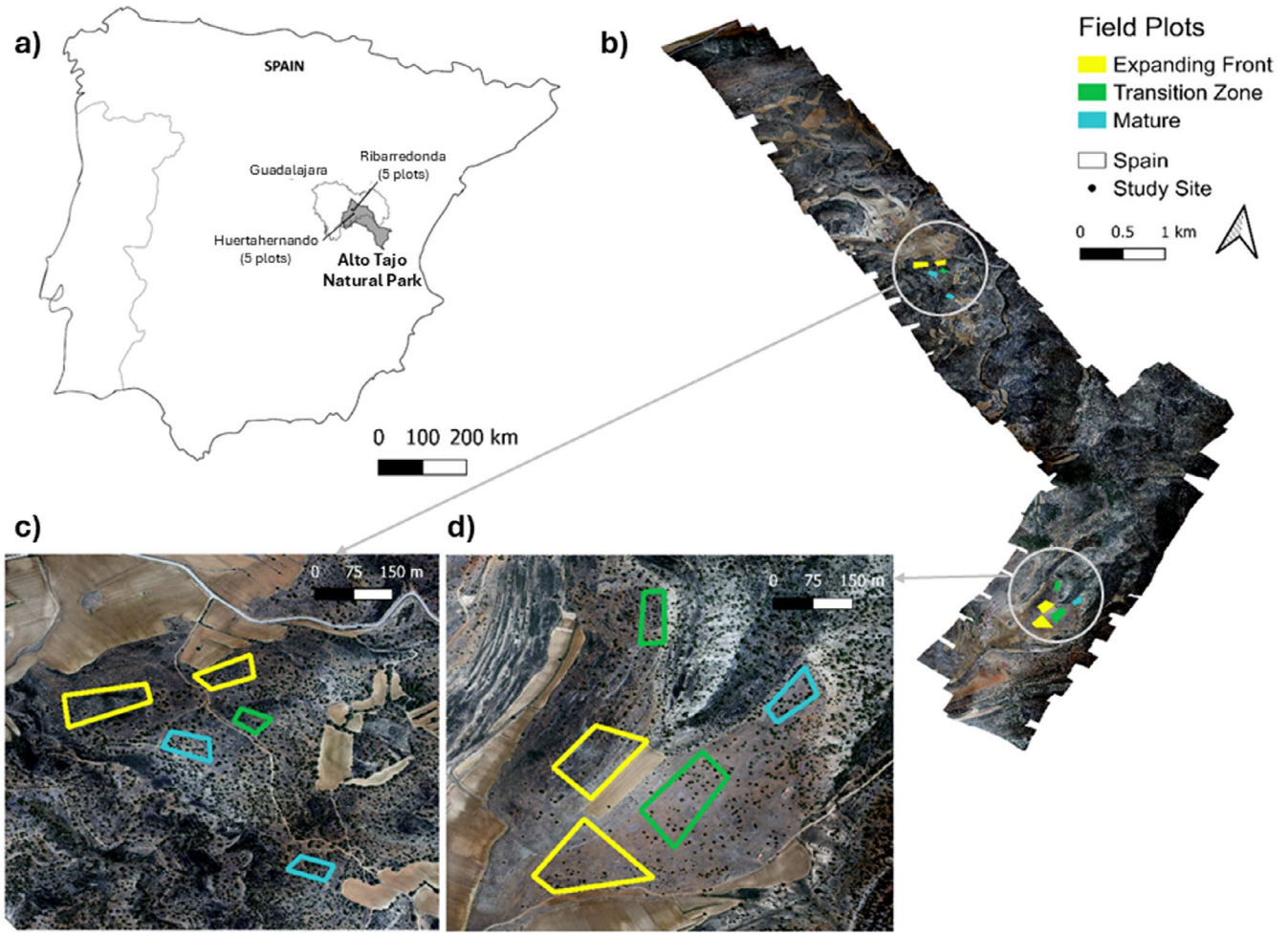

FIGURE 1 | Orthomosaic of the 20 km^2 of central Spain surveyed by aircraft in 2017 (a) Location of the orthomosaic in the Guadalajara province, and within the Alto Tajo Natural Park (grey area); (b) location of field plots near the towns of study (c) Ribarredonda and (d) Huertahernando. The 10 field plots varied in the stage of juniper succession. Colours of the polygons represent the stage of the juniper expansion: blue = mature forest stands with a core of well-conserved forest; yellow = front of forest expansion on formerly abandoned agricultural lands; and green = transition zone between the two former stages.

2 | Materials and Methods

2.1 | Study Site

We conducted this study over 20 km^2 in Alto Tajo Natural Park, central Spain, near Huertahernando and Ribarredonda (Guadalajara province, −2.27 E, 40.85 N). The region features low-density vegetation, dominated by monospecific *J. thurifera* woodland (Figure 1). Common shrubs include *Genista scorpius* L. (DC.); *Prunus spinosa* L.; *Rosa canina* L.; *Juniperus oxycedrus* L. and *Thymus* and *Lavandula* species. Agricultural activities in the area included unirrigated wheat farming and low-density grazing for millennia (https://alto-tajo.com/), but these were largely abandoned since the 1960s due to widespread migration towards urban centres (Martín-Forés et al. 2020). The region has a dry, continental Mediterranean climate (mean annual temperature: 10.3°C, range: −28°C to 38°C, mean annual precipitation: 490 mm) with a summer drought (AEMET, n.d. data, 1961–2014) typically spanning 4 months, from June to September, according to Walter & Lieth's climate diagram of the area of study. Soils are haplic calcisols over karstified limestone with areas of siliciclastic rocks and coarse sediment (Andreas and Duscher 2019; European Commission 2005). Altitudes range from 962 m to 1239 m.

We established 10 plots representing three stages of Spanish juniper expansion: three plots were in mature forest stands (a core of well-conserved forest), four plots near the front of forest expansion (on abandoned agricultural lands) and three plots in a transition zone between the two former stages. Plots located across Huertahernando and Ribarredonda averaged 0.9 ± 0.6 SD ha, each with 44.7 ± 6.8 SD juniper trees. The study addressed forest growth at landscape, stand and individual tree scales (Figure 2).

2.2 | Land Cover Classification Over Time (1984–2018)

We developed a land cover classification for the 2100-km^2 region within the United Nations Educational, Scientific and Cultural Organization (UNESCO) World Geopark Molina Alto Tajo, encompassing the core and surrounding areas of the Alto Tajo Natural Park. This region combines strictly protected areas

16541103, 2026, 3, Downloaded from https://onlinelibrary.wiley.com/doi/10.1111/jvs.70142 by ALICIA FORNER - Spanish Cochrane National Provision (Ministerio de Sanidad) , Wiley Online Library on [04/05/2026]. See the Terms and Conditions (https://onlinelibrary.wiley.com/terms-and-conditions) on Wiley Online Library for rules of use; OA articles are governed by the applicable Creative Commons License

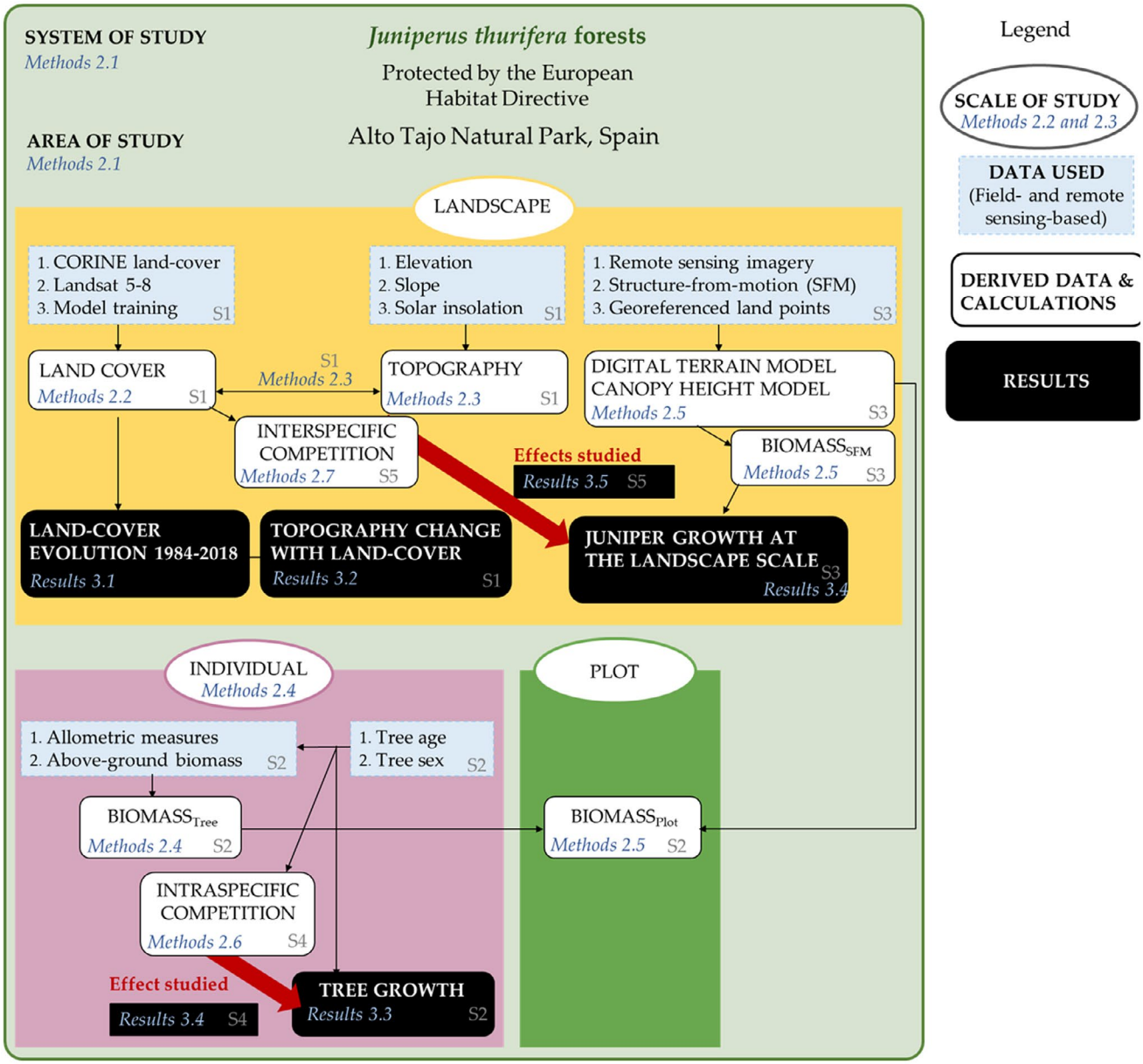

FIGURE 2 | Methodological diagram.

with their broader ecological context, including the Alto Tajo Natural Park (~1762 km^2), the Special Protection Area Alto Tajo (~1912 km^2), the Site of Community Importance Alto Tajo (~1401 km^2) and the surrounding Peripheral Protection Zone (~700 km^2). The area is ecologically rich, hosting a mosaic of Mediterranean forests, riparian woodlands and diverse habitats that support high biodiversity. By encompassing both the protected core and its buffer zones, we can develop a classifier for the Spanish juniper woodland and the various land cover classes that may have existed at the study site in the past.

To classify contemporary and historic land cover classes, we extracted multispectral Landsat 5–8 Tier 1 surface reflectance data of the region for 1984–2018. Landsat satellites 5–8 collected global, multispectral information from 1984 to the present at a 30-m resolution. We extracted data that had been atmospherically corrected using LEDAPS (Schmidt et al. 2013) from six Landsat bands (blue, green, red, near-infrared, shortwave infrared 1 and shortwave infrared 2, wavelengths are given in Appendix S1) from scenes with cloud cover less than 20% and a solar zenith angle less than 70° via Google Earth Engine. We masked any remaining clouds and cloud shadows using masks provided by the United States Geological Survey (USGS) associated with each scene and omitted any scenes with visible artefacts from subsequent processing. We then assembled image composites for two periods per year, approximately corresponding to summer (May– July) and winter (November–January), to capture intra-annual variation in land cover appearance. Additionally, we derived slope and aspect from the Spanish national DTM at a 5-m resolution (MDT05 2009 CC-BY 4.0 scne.es, www.ign.es) and aggregated them to match the Landsat imagery resolution. See Appendix S1 for further information on data selection and pre-processing.

To enable training and validation of a random forest classifier, we generated 500 randomly located points in the 2100-km^2 region

16541103, 2026, 3, Downloaded from https://onlinelibrary.wiley.com/doi/10.1111/jvs.70142 by ALICIA FORNER - Spanish Cochrane National Provision (Ministerio de Sanidad) , Wiley Online Library on [04/05/2026]. See the Terms and Conditions (https://onlinelibrary.wiley.com/terms-and-conditions) on Wiley Online Library for rules of use; OA articles are governed by the applicable Creative Commons License

around Alto Tajo Natural Park and manually classified them into four land cover classes—agriculture, grassland and dwarf shrubland, woodland and shrubland, and closed forest, following the CORINE system (European Environment Agency 2019) and associated regional studies (Corbane et al. 2015; Shoshany 2000; Yüksel et al. 2008) (see Appendix S1 for land class definitions). We used high-resolution satellite imagery available on Google Earth Pro (30–50 cm resolution, acquired by CNES/AIRBUS) to assign the land class in a 30 m^2 buffer around each point. Each point was classified for multiple years where data were available (2004–2018). Where available for a given point and year, Google Street View imagery was used as a secondary imagery source to support manual classification for a point. Manual classifications affected by incomplete satellite image coverage, cloud cover and urban areas (due to their extremely low total coverage) were dropped from the training and validation. This resulted in 673 classifications of 409 spatially unique points. Additional quality controls for this process are described in Appendix S1.

We trained a Random Forest classifier on a stratified random sample of 70% of the spatially unique reference points, stratified on modal land class per point across multiple years. The model predicted land cover using slope, aspect, the six extracted Landsat bands, and the normalised difference vegetation index (indicator of vegetation presence; Rouse et al. 1974) for both summer and winter periods. The random forest classifier was trained over 300 trees with a bag fraction of 0.7 and a minimum leaf population of 3. The remaining reference points (30%) were used for validating the classifier by comparing manually classified points to those in the land cover map in the relevant year. We calculated the overall cross-validation accuracy and the producers and consumers accuracy for the identification of each land cover class individually, resulting in an overall cross-validation accuracy of 74% (see Appendix S1 for accuracy per class). To confirm that variation in Landsat bandwidths between Landsat 8 and 7 did not impact the classifier, a second hindcasting validation was performed using training points from 2014 to 2018 only, validated against a subset of validation points that fell between 2004 and 2013, resulting in a similar cross-validation accuracy of 71.4 (Appendix S1).

2.3 | Link Between Land Cover and Topography

To identify environmental drivers of woodland expansion, we analysed how rates of change for each land-cover class were related to topography (see Appendix S1 for details). Specifically, we considered elevation (m), slope (degrees) and annual solar insolation ($kW.m^{-2}\,year^{-1}$). We estimated mean rates of land cover class change using linear regressions of area over time, running separate models followed by an ANOVA *F*-test for each land cover class. We found no residual temporal autocorrelation. We tested for systematic changes in land cover classes in relation to elevation, slope and solar insolation using quantile regression. We used quantile regression to understand how the distributions of land cover classes had shifted across the landscape over time and to test for systematic changes in relation to elevation, slope and solar insolation (Koenker 2004). For each response variable (elevation, slopes and irradiance), we modelled the distribution of each land cover class as a function of year, using the 90th, 75th, 50th, 25th and 10th quantiles to capture trends across different extremes. We used the R package quantreg (Koenker et al. 2019) to assess the significance of age-related trends and determine if model functions differed across quantiles using Wald tests (Koenker and Bassett 1982). We estimated standard errors in rates of change using Markov chain marginal bootstrapping (He and Hu 2002; Kocherginsky et al. 2005).

2.4 | Juniper Growth Measurements at the Individual Level

We collected data on tree biomass and juniper growth for 447 individual junipers across the 10 plots at our study site, shown in Figure 1 (see Appendix S2 for details). Each tree was georeferenced using a differential geographic positioning system and surveyed for height, stem diameter at breast height (used to calculate tree quadratic diameter, QD), basal area, sex and crown diameter (average of two perpendicular measurements) between June and October 2017. We estimated above-ground biomass for each individual from these measurements, using allometry equations specific to *J. thurifera* (Ruiz-Peinado et al. 2011) (see Appendix S2 for more details). Additionally, we measured tree age by extracting wood cores in a random sample of 30 trees per plot and counting and measuring ring widths, totalling estimates for 251 individuals (see Alfaro-Sánchez, Espelta, Valladares, et al. 2021; Alfaro-Sánchez, Espelta, Acuña-Míguez, et al. 2021 for methodological details on tree age and dataset).

2.5 | Mapping Juniper Growth at the Plot and Landscape Levels

We aggregated tree-level biomass ($Biomass_{Tree}$) to determine aboveground biomass density ($Biomass_{Plot}$, $Mg\,ha^{-1}$) in the 10 field plots shown in Figure 1 (see Appendix S2). Previous studies demonstrate that aboveground biomass of Mediterranean woodlands can be estimated robustly from maps of canopy height, using mean top of canopy height and canopy fraction as explanatory variables extracted from these maps (García et al. 2010; Jucker et al. 2017; Galidaki et al. 2017; Simonson et al. 2015). Airborne lidar is the preferred approach to measuring top of canopy height in dense forests, but in open juniper woodlands, it is equally effective to develop a canopy height map from high-resolution photographic imagery by applying a structure-from-motion (SFM) technique. We surveyed 19.6 km^2 with an aircraft to get images at a resolution of 9.48 cm $pixel^{-1}$ (see Appendix S3 for details). We orthorectified the digital imagery and processed it using Agisoft Photoscan, to produce a structure-from-motion-derived point cloud with over 160 million points, with an average point density of 8.42 m^{-2}, and a location error of 0.24 m (longitude/latitude) and 0.58 m (altitude). We then created a digital terrain model and canopy height model at a 1-m resolution using lastools (Isenburg 2019). We identified ground points after first excluding those in deep shadow, associated with higher degrees of uncertainty in photogrametry (red 0–45; green 0–55; blue 0–70) and secondly by excluding green pixels typical of *J. thurifera* (green 0–150) to avoid misclassifying small trees as terrain, where the base of the canopy is close to the ground and photogrammetry had not produced ground points under the tree. These thresholds were identified to reliably distinguish areas with large amounts of vertical noise (shadow) and juniper trees from the

16541103, 2026, 3, Downloaded from https://onlinelibrary.wiley.com/doi/10.1111/jvs.70142 by ALICIA FORNER - Spanish Cochrane National Provision (Ministerio de Sanidad) , Wiley Online Library on [04/05/2026]. See the Terms and Conditions (https://onlinelibrary.wiley.com/terms-and-conditions) on Wiley Online Library for rules of use; OA articles are governed by the applicable Creative Commons License

surrounding landscape through repeat testing across the surveyed landscape. Green pixels were restored after ground point identification and prior to any subsequent processing of canopy height or canopy fraction. We gap-filled the data (<0.6% of the area) by interpolating from up to 10 adjacent pixels and normalised point altitudes relative to terrain height to derive the canopy height model (Isenburg 2014; Khosravipour et al. 2014). We manually masked areas of terrain incorrectly labelled as canopy due to significant elevation changes (0.06% of the area). We calculated the mean top of canopy height and canopy fraction (the percentage area with a tree height over 0.5 m) for each plot and across the landscape at a 26.9-m resolution, using only tree crown pixels (>0.5 m).

We compared models of biomass (estimated from field data) as a function of either top of canopy height, canopy fraction or the interaction between the two and carried out a leave-one-out regression on log-transformed data of the biomass at the plot level ($Biomass_{Plot}$) to select the best-performing model for predicting biomass at the landscape scale. The model with the lowest percentage bias, root mean squared error (RMSE) and mean absolute error (MAE) was selected to predict landscape biomass ($Biomass_{SFM}$) within pixels over an area of 4.3 km^2 which was identified as being monospecific *J. thurifera* in the field. Analyses were performed in R 3.6.1 (R Core Team 2021) (see Appendix S3 for details).

2.6 | Effect of Intraspecific Competition on Juniper Growth at an Individual Tree Scale

We investigated the effect of intraspecific competition on juniper growth using mixed-effect models. We modelled the biomass of individual trees as a function of age and sex, and as a function of local competition with neighbouring juniper trees. Specifically, we used Hegyi's competition coefficient to quantify the competitive impact of neighbouring trees based on the distribution of crown projection sizes, which approximates an individual's sphere of influence (Hegyi 1974; Schenk and Jackson 2002; see Appendix S4 for more details). To evaluate the neighbourhood size that was most appropriate, we calculated Hegyi's index within circles of 10, 15 and 20 m and selected the best-performing model using Akaike information criterion (AIC). We assessed variable significance using Wald confidence intervals. Models were fitted to a stratified random sample of 70% of field-measured trees (177 trees). The remaining 74 trees validated the model and helped calculate an antilogarithmic correction factor (1.29), which we applied to all model predictions. Fixed-effect prediction intervals were estimated using 1000 coefficient estimates drawn randomly from the model's covariance matrix.

2.7 | Effects of Topography and Interspecific Competition on Juniper Growth at the Landscape Scale

We investigated the effects of topography on juniper biomass accumulation rates at the landscape scale to assess the influence of this driver on the natural colonisation process. We used a space-for-time substitution to account for stand age on biomass, using age variation in the landscape calculated in woodland patches from land cover classifications. We also used values for elevation, slope and solar insolation previously calculated (see Appendix S5 for details).

We included shrub cover in the model to investigate interspecific competition's impact on growth at the landscape scale. Shrub cover was defined as the presence of dwarf shrubland surrounding junipers, within each 30 m pixel used in the analysis and was manually classified as low, medium or high for each pixel using the orthorectified RGB imagery collected in 2017. The most prominent species of the dwarf shrubland surrounding juniper trees was *Genista scorpius* (L.) DC., *Prunus spinosa* L., *Rosa canina* L., *Thymus* sp. and *Lavandula latifolia* Medik. ex Vill. Associations between the distribution of dwarf-shrub cover and both age and topographically derived variables were ruled out using an ordination (see Appendix S5 for details).

We employed a spatial simultaneous autoregressive error model (Kissling and Carl 2008) using the R package *spatialreg* (Bivand et al. 2013) to account for local spatial autocorrelation in $Biomass_{SFM}$, identified via Moran's I (Moran 1948). We used a square-root transformation to satisfy normality assumptions. We selected the neighbourhood size best explaining spatial autocorrelation of $Biomass_{SFM}$ by comparing maximal model structure AIC with increasing neighbourhood sizes (50 increments of 20 m) from the threshold identified by Moran's I. We then confirmed no significant residual spatial autocorrelation (Moran's I standard deviate: 0.53, $p = 0.30$). For the model of $Biomass_{SFM}$, we selected the best model structure with the lowest AIC. We assessed variable significance using the likelihood ratio test for spatial linear models within the *spatialreg* R package. We estimated effect-size confidence intervals by drawing 1000 coefficient estimates randomly from the model's covariance matrix, in the absence of spatial dependence.

3 | Results

3.1 | Land Cover Evolution From 1984 to 2018

Land cover changed substantially over the 34-year study period (Figure 3). There was an accentuated decline in agricultural land, which occupied 33.5% of the study area in 1984 but only 8.1% in 2018 (annual loss rate: 0.75%). The decline was also observed in grassland + dwarf-shrubland area, which occupied 50.4% and 40.2% of the area of study, respectively, in 1984 and 2018 (annual loss rate: 0.3%). This decline in agricultural and grazed lands was accompanied by the noticeable expansion of open woodland + shrubland area that increased from 16% to 47% over this period (annual gain rate: 0.91%), and of closed forests that increased from 0.1% in 1984 to 2.2% in 2018 (annual gain rate: 0.06%). Closed woodlands remained a small component of the landscape. Abandoned croplands had transitioned largely to grassland by 2018. Most new woodland colonised previous grasslands.

3.2 | Changes in the Topographic Distribution of Land Cover Classes Over Time

The topographic distribution of land cover classes shifted over the 34-year study. The rate of change in the distribution of land cover over elevation (m), slope (degree) and annual solar insolation

16541103, 2026, 3, Downloaded from https://onlinelibrary.wiley.com/doi/10.1111/jvs.70142 by ALICIA FORNER - Spanish Cochrane National Provision (Ministerio de Sanidad) , Wiley Online Library on [04/05/2026]. See the Terms and Conditions (https://onlinelibrary.wiley.com/terms-and-conditions) on Wiley Online Library for rules of use; OA articles are governed by the applicable Creative Commons License

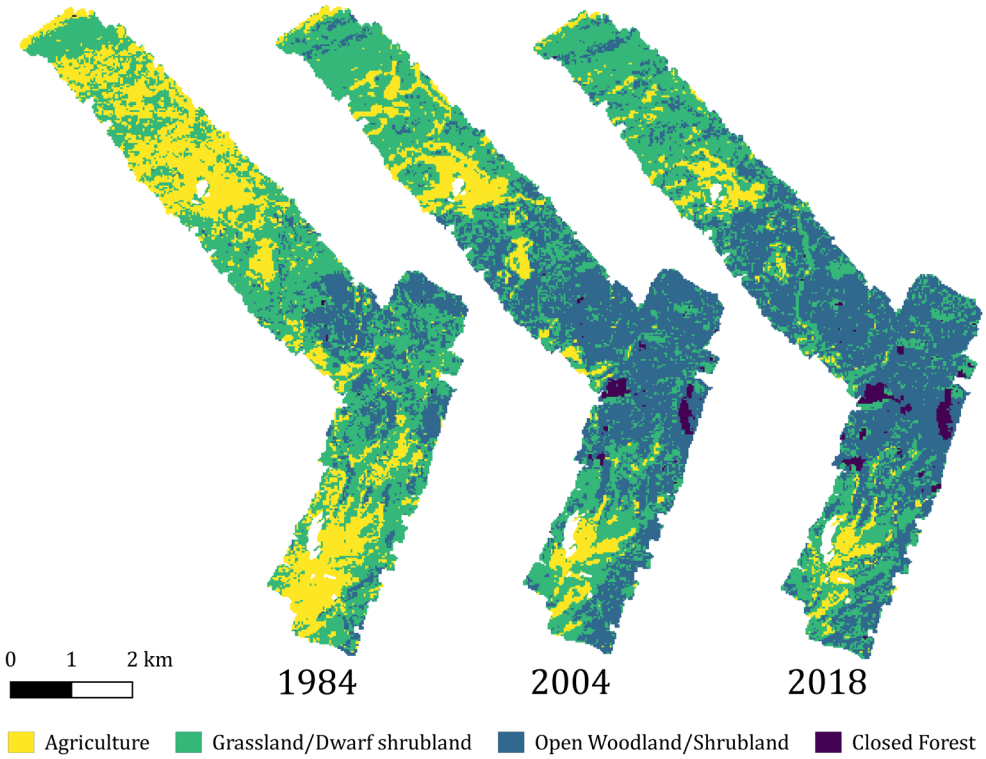

FIGURE 3 | Land cover maps for the years 1984, 2004 and 2018 for a 20-km^2 region in central Spain, derived from Landsat imagery via a random forest model and a manually classified training dataset. Annual time series of land cover change for the period 1984–2018 were used in analyses.

(kW.m^{-2}year^{-1}) differed significantly across the quantiles of the distribution for all models (Figure 4). The four classes of land cover are broadly stratified by slope. Initially, agricultural land occupied the shallowest slopes, but tree cover increased as the slope increased. Agricultural land on the steepest occupied slopes was preferentially abandoned, and the rate of abandonment was least on shallow slopes (i.e., the 10th quantile of the land-cover distribution with respect to slope) and greatest on the steepest slopes (i.e., 90th quantile; Figure 4). The expansion of woodland and closed forest went into less steep regions previously occupied by grasslands. The median elevation of woodland decreased a small but significant amount, a trend that was consistent across quantiles. The elevation of grassland increased substantially, occupying a similar distribution to the remaining agriculture by 2018 (Figure 4). Woodland occupies areas that experience more extreme values of annual solar insolation, compared to grassland or agriculture, but over the 34-year period studied, median insolation decreased and the distribution of woodland across solar insolation became more centrally weighted (Figure 4). Appendix S1 provides further details of these analyses.

3.3 | Juniper Growth at the Individual Scale and Effects of Sex and Intraspecific Competition

The above-ground biomass of individual juniper trees increased significantly as a function of age determined from tree rings (Wald interval: 2.5% = 0.04, 97.5% = 0.06) and with reduced competition from neighbours (Hegyi coefficients ($H_{20\text{-}m}$) = −0.08, with 95% CI −0.10 to −0.06). This shows that junipers in proximity to other, large individuals accumulated significantly less biomass for their age, and that intraspecific competition is strongly size asymmetric (Figure 5). No effect of sex was found on tree biomass (see Appendix S4 for details on model selection).

3.4 | Spanish Juniper Growth Within Field Plots Across the Landscape Scale

Aboveground biomass estimated from individual tree measurements in the 11 field plots ranged from 1.2–27.2 Mg ha^{-1} and, as expected, was greater in mature forests than early stages of colonisation ($X^2 = 7.44$, $p = 0.02$). The best-performing model for predicting landscape biomass ($Biomass_{SFM}$) was $Biomass_{SFM} = 32.9 \times 1.11\ (\text{Top of canopy height} \times \text{canopy fraction})^{0.62}$, when converted back to the native scale (see Appendix S3 for details on calculations).

Very little bias or error was found between estimates of $Biomass_{SFM}$ at different resolutions (26.9–80.6 m: RMSE = 0.32, bias = 2.42%, MAE = 0.03; 26.9–107.5 m: RMSE = 0.39, bias = 2.64%, MAE = 0.02).

Our estimates show that the average biomass of juniper woodland in the landscape was 14.7 Mg ha^{-1}, with an interquartile range from 8.1 Mg ha^{-1} to 20.1 Mg ha^{-1}. Woodland biomass increased significantly with age (likelihood ratio = 68, df = 3, $p < 0.0001$) (see Appendix S3 for details on calculations and alternative modelling approaches that were explored but rejected).

16541103, 2026, 3, Downloaded from https://onlinelibrary.wiley.com/doi/10.1111/jvs.70142 by ALICIA FORNER - Spanish Cochrane National Provision (Ministerio de Sanidad) , Wiley Online Library on [04/05/2026]. See the Terms and Conditions (https://onlinelibrary.wiley.com/terms-and-conditions) on Wiley Online Library for rules of use; OA articles are governed by the applicable Creative Commons License

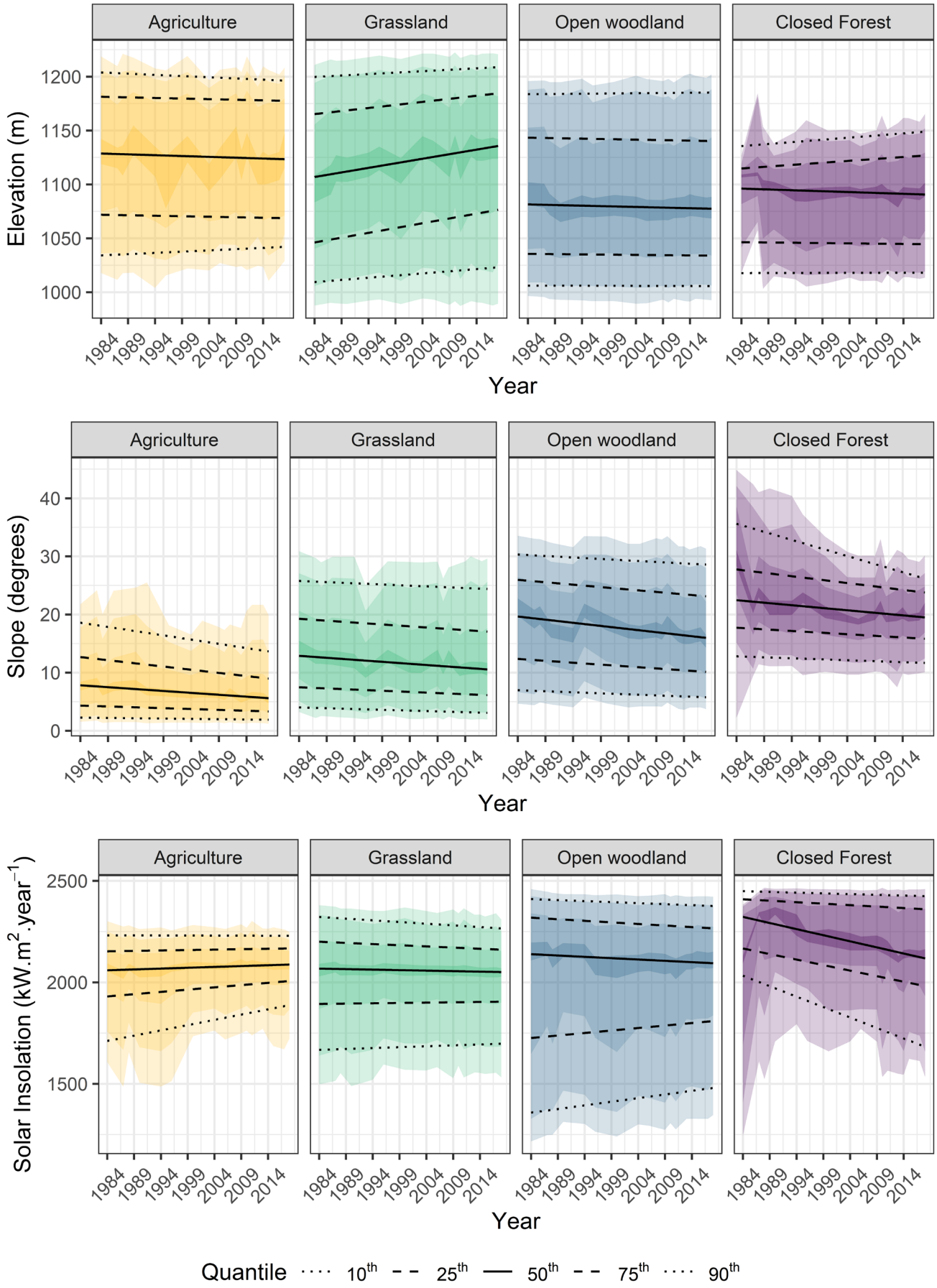

FIGURE 4 | Legend on next page.

16541103, 2026, 3, Downloaded from https://onlinelibrary.wiley.com/doi/10.1111/jvs.70142 by ALICIA FORNER - Spanish Cochrane National Provision (Ministerio de Sanidad) , Wiley Online Library on [04/05/2026]. See the Terms and Conditions (https://onlinelibrary.wiley.com/terms-and-conditions) on Wiley Online Library for rules of use; OA articles are governed by the applicable Creative Commons License

FIGURE 4 | Long-term trends in the elevation (a), slope (b) and solar insolation (c) of sites occupied by agriculture, grasslands, open woodlands and closed woodlands in a 20-km^2 region of central Spain undergoing land-use change. Shifts in the distribution of land cover types across terrain in the region of Huertahernando and Ribarredonda, estimated by quantile regression at the 10th, 25th, 50th, 75th and 90th quantiles. Data distribution is shown via the 5th–95th, 10th–90th, 25th–75th and 45th–55th quantiles for each land cover classification. The mean trendline is shown in bold, while upper and lower limits are shown as dotted lines (5th and 95th percentiles). Shaded areas represent the distribution of data.

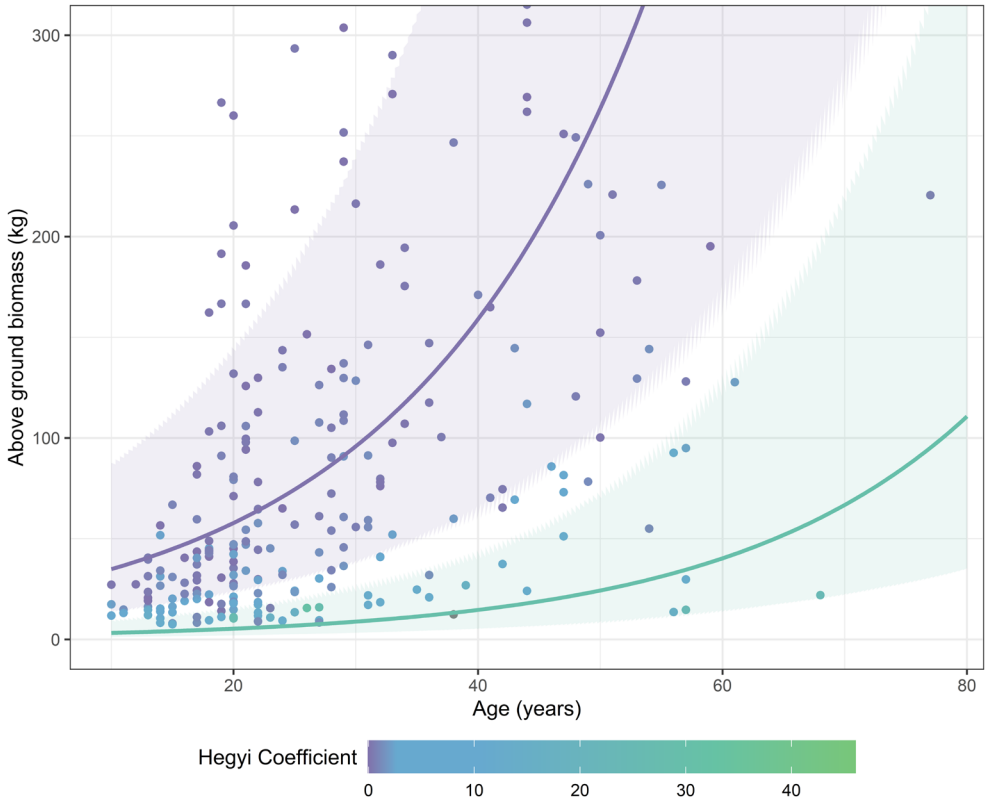

FIGURE 5 | Estimated aboveground biomass for individual *J. thurifera* trees as a function of the age determined from tree rings and neighbourhood competition (assessed by the Hegyi competition coefficient). The model was $ln(\text{Biomass}) = 2.786 + 0.051\ \text{Age} - 0.080\ H_{20}$. Predictions of biomass as a function of age (with 95% CIs) are shown when the Hegyi coefficient is set at 0 and 30.

3.5 | Effect of Topography and Interspecific Competition on Juniper Growth at the Landscape Scale

We found that abandoned lands at higher elevation had lower biomass when initially classified as woodland (likelihood ratio = 69, df = 1, $p < 0.0001$; Figure 6a). However, elevation in this hilly landscape did not have a significant effect on the rate of biomass accumulation over the 30 years following (Age × elevation: likelihood ratio = −0.47, df = 1, $p = 0.49$). The rate of increase in biomass with age was significantly higher where solar insolation was high (likelihood ratio = 16, df: 1, $p < 0.0001$). However, newly established woodland contained significantly more biomass where insolation was low, suggesting that the effects of sun exposure varied with stand age (Figure 6b). Changing vulnerabilities may be due to microclimatic or physiological changes associated with stand age, differing soil properties across the expansion gradient, or may also reflect changing climatic conditions over the last 30 years, as a product of the space-for-time substitution. Regarding interspecific competition at the landscape scale, our results show that a greater density of dwarf shrubland led to lower biomass at woodland establishment (likelihood ratio = 103, df = 2, $p < 0.0001$) but did not have a significant effect on the rate of accumulation over the 30 years following (Age × shrubland cover: likelihood ratio = −1.5, df = 2, $p = 0.47$; Figure 6c). The Nagelkerke pseudo-R^2 of the best supported model was 0.21 and the plot random effect explained 34% of biomass variation (see Appendix S5 for coefficient estimates of the model).

4 | Discussion

Over the past three decades, *J. thurifera* woodlands in central Spain have considerably expanded, primarily into flatter areas released by agricultural abandonment. Our analyses show that this expansion is shaped by a combination of abiotic conditions, competition and land-use legacies. High irradiance accelerated biomass accumulation over time but constrained growth in newly established stands, while denser juniper and shrub layers reduced individual biomass, particularly in more mature stands. These findings demonstrate that contemporary competition and environmental heterogeneity, rather than historical disturbances alone, govern growth dynamics and the pace of Spanish

16541103, 2026, 3, Downloaded from https://onlinelibrary.wiley.com/doi/10.1111/jvs.70142 by ALICIA FORNER - Spanish Cochrane National Provision (Ministerio de Sanidad) , Wiley Online Library on [04/05/2026]. See the Terms and Conditions (https://onlinelibrary.wiley.com/terms-and-conditions) on Wiley Online Library for rules of use; OA articles are governed by the applicable Creative Commons License

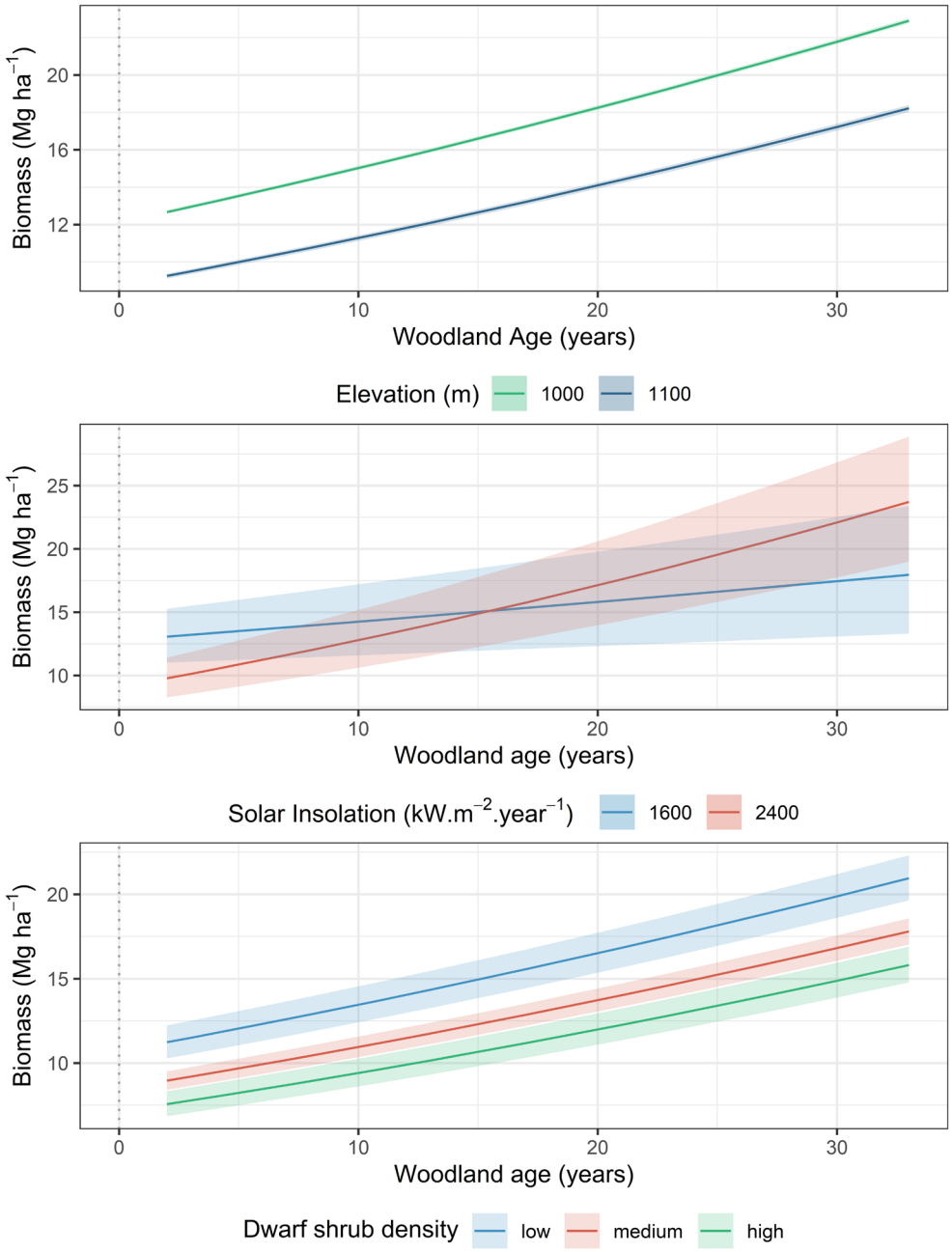

FIGURE 6 | Predicted accumulation of aboveground biomass over time within *J. thurifera* patches, and the influence of elevation (a), insolation (b) and interspecific competition with dwarf shrubs (c) on that biomass growth. 'Time' on the *x*-axis is years since a site was first colonised by juniper (woodland age, assessed by land-cover change analyses). Model predictions and 95% confidence intervals are shown. The biomass model with the greatest statistical support was: Sqrt (Biomass) ~ Age + Slope + Elevation + Solar + Shrub cover + (Age × Slope) + (Age × Elevation) + (Age × Solar) + (Age × Shrub cover).

juniper woodland expansion. The following subsections explore in depth (i) land-cover evolution, (ii) the role of intraspecific competition and (iii) the role of topography and interspecific competition in structuring juniper growth across scales.

4.1 | Evolution of Land Cover Over the 34 Years of Study, Including Juniper Expansion

Woodland expanded into abandoned farmland across Alto Tajo Natural Park, as observed across many areas of Southern Europe (Peña-Angulo et al. 2019; Hampe et al. 2020). They expanded out from steep, sun-exposed slopes into previously cultivated areas as farming lost its economic viability (Weissteiner et al. 2011; Lasanta-Martínez et al. 2005; Navarro and Pereira 2015). While woodlands established mostly in former grazing lands, likely due to greater opportunities for establishment and subsequent densification, young junipers have also appeared in ex-arable zones (Acuña-Míguez et al. 2020; Gimeno, Escudero, et al. 2012; Gimeno, Camarero, et al. 2012; Martín-Forés et al. 2022). By combining remote sensing and field-based measurements, we find that the aboveground biomass of Spanish juniper increased

16541103, 2026, 3, Downloaded from https://onlinelibrary.wiley.com/doi/10.1111/jvs.70142 by ALICIA FORNER - Spanish Cochrane National Provision (Ministerio de Sanidad) , Wiley Online Library on [04/05/2026]. See the Terms and Conditions (https://onlinelibrary.wiley.com/terms-and-conditions) on Wiley Online Library for rules of use; OA articles are governed by the applicable Creative Commons License

with successional stage, providing insights into the recovery of this priority habitat. While our study focused on aboveground biomass, future research should include belowground biomass and carbon dynamics to fully assess the carbon sequestration capacity of juniper woodlands (Addo-Danso et al. 2016).

4.2 | Role of Intraspecific Competition on Tree Juniper Growth

Our exploration of alternative models emphasizes the importance of understanding multiple factors in natural woodland expansion. Biomass accumulation was sensitive to competition with conspecifics at the individual level, particularly in dense stands (i.e., Hegyi competition coefficients >25), consistent with previous studies based on annual tree ring widths (Alfaro-Sánchez, Espelta, Valladares, et al. 2021). Given the age distribution of studied individuals and the well-documented capacity of *J. thurifera* to recover from historic growth suppression (Olano et al. 2008), it is unlikely that variation in individual above-ground biomass could be due to historic browsing suppression (DeSoto et al. 2010; García Morote et al. 2012). This suggests that the observed intraspecific growth patterns are more likely driven by present-day competition dynamics rather than legacy effects of past disturbances by herbivores. Reduced growth has also been observed in individuals of other resprouting, multi-stemmed species, attributed to increased light competition amongst stems (Espelta et al. 2003) and competition for belowground resources (Coomes and Grubb 2000). Such competitive effects align with the stress-tolerant strategy of *J. thurifera*, which favours persistence under harsh conditions but amplifies resource limitation in dense stands. Indeed, Acuña-Míguez, Valladares and Martín-Forés et al. (2020) reported higher water-use efficiency at expanding fronts and reduced growth in mature, denser woodlands. Actively managing juniper stand density may be a viable option to alleviate intraspecific competition and foster healthier and more productive juniper woodlands, with the potential for enhanced growth and biomass accumulation in the remaining trees.

4.3 | Topography and Interspecific Competition as Crucial Factors in Juniper Growth Population

Juniper annual growth patterns are sensitive to drought stress (Alfaro-Sánchez, Espelta, Valladares, et al. 2021), which is in turn influenced by sun exposure, competitive impacts of dwarf shrubs and legacies of agriculture on nutrient supply. We found that high solar radiation had a negative impact on young junipers but supported high-biomass mature stands. These mature stands are characterised by extensive root systems that access deeper water reserves and provide microclimatic buffering and shading (Niinemets 2010), making them more resilient to heat, high solar radiation and drought stress, potentially enabling higher rates of photosynthesis with the same insolation. However, older stands also began accumulating carbon decades earlier than the youngest stands in our study and will not have been affected by climate change and increasing drought stress in the same way. Climate change has resulted in a higher frequency of hot days and dry conditions in the Iberian Peninsula since the 20th Century (Intergovernmental Panel on Climate Change (IPCC) 2023; Lindner et al. 2010) and may have affected the suitability of more exposed sites for Juniper in the region, increasing the relative impact of solar insolation growth. Unpicking the relative importance of recent climate change and increased resilience with age on growth rates requires further investigation. We also found that higher densities of dwarf shrubs were correlated with lower biomass for junipers of the same age, suggesting that competition for nutrients and water is a limiting factor in areas with greater shrub cover (DeSoto et al. 2010; Montesinos and Fabado 2015). While recruitment can benefit from heterospecific cover in extreme conditions (Martín-Forés et al. 2022), our findings showed that once woodland is established, dwarf shrubland negatively impacts biomass. This interspecific competition might overshadow the positive effects seen during the recruitment phase. Our results indicate that competition with other species causes similar variations in woodland biomass as abiotic stressors like topographical changes. Resilience to drought is also influenced by agricultural legacies. In abandoned agricultural sites, higher nutrient availability promotes relatively fast growth of young juniper stands under low drought stress, but this growth advantage comes at the cost of increased vulnerability to more intense droughts (Alfaro-Sánchez, Espelta, Valladares, et al. 2021).

5 | Implications for Conservation

By combining land cover mapping over 34 years with field-based measurements and structure-from-motion analyses, our study revealed significant expansion of juniper woodlands in abandoned agricultural land. Woodland expansion is linked to topography and sun exposure. Rapid growth of new juniper stands in more shaded sites may have benefited from these lands having been cultivated and enriched with nutrients in the past. Junipers were significantly affected by intra- and interspecific competition, with greater densities of dwarf shrubland within stands negatively impacting juniper biomass at the landscape scale. This suggests different constraints on growth may be acting on the expanding front of the woodland and demonstrates the importance of local competition and abiotic conditions for expanding growth, acting over large spatial scales and multi-decadal time scales. Beyond our regional focus, our integrative framework—combining airborne photogrammetry, long-term land cover analysis and field-based biomass models—offers a scalable and transferable approach to study vegetation dynamics across broader spatial and temporal scales. This novel and comprehensive methodology could be readily applied to other study areas to monitor natural regeneration and assess the efficacy of restoration efforts in other ecosystems. Likewise, it could be implemented to study climate-driven vegetation shifts, thereby enhancing large-scale conservation and management planning under future climate conditions.

We suggest experimenting with mechanical shrub clearance or controlled grazing to reduce the long-term colonisation and dominance of these priority habitats by competing woody species (Castro et al. 2004; DeSoto et al. 2010; Smit et al. 2008). Implementing combined silvicultural and soil management practices across these expanding woodlands could also improve water retention, nutrient availability and soil structure

16541103, 2026, 3, Downloaded from https://onlinelibrary.wiley.com/doi/10.1111/jvs.70142 by ALICIA FORNER - Spanish Cochrane National Provision (Ministerio de Sanidad) , Wiley Online Library on [04/05/2026]. See the Terms and Conditions (https://onlinelibrary.wiley.com/terms-and-conditions) on Wiley Online Library for rules of use; OA articles are governed by the applicable Creative Commons License

(Binkley and Fisher 2019), thereby benefiting juniper trees over the woody species growing in their vicinity. Carefully tailored management strategies could enhance the resilience of Spanish juniper to future abiotic stressors, such as climate change.

Author Contributions

D.A.C. and I.M.-F. are co-senior, and equally contributing, authors. Conceptualization, methodology, software and validation: all authors; formal analysis: L.B.; investigation: L.B., A.F., I.M.-F. and S.K.; resources: L.B., A.F., I.M.-F. and S.K.; data curation: L.B., A.F. and I.M.-F.; manuscript writing: L.B., A.F. and I.M.-F.; review and editing: all authors; visualisation: D.A.C., A.F., I.M.-F. and F.V.; supervision: D.A.C., I.M.-F. and F.V.; project administration: D.A.C.; funding acquisition: D.A.C. and F.V. All authors have read and agreed to the published version of the manuscript.

Acknowledgements

We would like to thank the NERC Airborne Research Facility for the collection of remote sensing data in 2017 (project code ES17/126), the NERC Geophysical Equipment Facility for the loan of equipment that made this research possible and NERC-ARF-DAN for the processing of digital imagery to an orthorectified mosaic and point cloud. We also want to thank D. López Quiroga, B. Acuña-Míguez, J. M. Olano, P. Álvarez García, E. Serna, M. Diaz-Carro, B. Ruiza-Valdepeñas, A. Escudero, E. Manrique and A. Bravo-Oviedo, for their valuable support in laboratory and field work. Open access publishing facilitated by Adelaide University, as part of the Wiley - Adelaide University agreement via the Council of Australasian University Librarians.

Funding

This research was funded by the Natural Environment Research Council (NERC), the Spanish Ministry of Economy and Competitiveness (MINECO) grant: 345 SPONFOREST (BiodivERsA3-2015-58, PCIN-2016-055), COMEDIAS (CGL2017-83170-R) and Comunidad de Madrid grant: REMEDINAL TE (Ref. TE-CM. S2018/EMT-4338, 347 2019-2023-Comunidad de Madrid). A.F. was supported by a JAE-predoc fellowship from the Spanish National Research Council (CSIC) and by an APOSTD fellowship from the Generalitat Valenciana and co-funded by the European Union.

Conflicts of Interest

The authors declare no conflicts of interest.

Data Availability Statement

Data collected in this work are publicly available via the CEDA Archive (airborne remote sensing imagery) and Zenodo (tree traits): NERC Airborne Research Facility (2026) and Bentley et al. (2026).

References

Acuña-Míguez, B., F. Valladares, and I. Martín-Forés. 2020. "Both Mature Patches and Expanding Areas of *Juniperus thurifera* Forests Are Vulnerable to Climate Change but for Different Reasons." *Forests* 11, no. 9: 1–13. https://doi.org/10.3390/f11090960.

Addo-Danso, S. D., C. E. Prescott, and A. R. Smith. 2016. "Methods for Estimating Root Biomass and Production in Forest and Woodland Ecosystem Carbon Studies: A Review." *Forest Ecology and Management* 359: 332–351. https://doi.org/10.1016/j.foreco.2015.08.015.

AEMET. n.d. "Agencia Estatal de Meteorología, Gobierno de España." https://www.aemet.es.

Alfaro-Sánchez, R., J. M. Espelta, B. Acuña-Míguez, F. Valladares, and I. Martín-Forés. 2021. "Disentangling the Role of Sex Dimorphism and Forest Structure as Drivers of Growth and Wood Density in Expanding *Juniperus thurifera* L. Woodlands." Figshare. https://doi.org/10.6084/m9.figshare.14806683.v1.

Alfaro-Sánchez, R., J. M. Espelta, F. Valladares, B. Acuña-Míguez, and I. Martín-Forés. 2021. "Disentangling the Role of Sex Dimorphism and Forest Structure as Drivers of Growth and Wood Density in Expanding *Juniperus thurifera* L. Woodlands." *Annals of Forest Science* 78, no. 4: 1–19. https://doi.org/10.1007/s13595-021-01097-6.

Alfaro-Sánchez, R., A. S. Jump, J. Pino, O. Díez-Nogales, and J. M. Espelta. 2019. "Land Use Legacies Drive Higher Growth, Lower Wood Density and Enhanced Climatic Sensitivity in Recently Established Forests." *Agricultural and Forest Meteorology* 276–277: 107630. https://doi.org/10.1016/j.agrformet.2019.107630.

Allen, H., W. Simonson, E. Parham, E. d. B. Santos, and P. Hotham. 2018. "Satellite Remote Sensing of Land Cover Change in a Mixed Agro-Silvo-Pastoral Landscape in the Alentejo, Portugal." *International Journal of Remote Sensing* 39, no. 14: 4663–4683. https://doi.org/10.1080/01431161.2018.1440095.

Andreas, G., and K. Duscher. 2019. *Extended Vector Data of the International Hydrogeological Map of Europe 1:1,500,000 (Version IHME1500 v1.2)*. Federal Institute for Geosciences and Natural Resources (BGR).

Astigarraga, J., E. Andivia, M. A. Zavala, et al. 2020. "Evidence of Non-Stationary Relationships Between Climate and Forest Responses: Increased Sensitivity to Climate Change in Iberian Forests." *Global Change Biology* 29, no. 9: 5063–5076. https://doi.org/10.1111/gcb.15198.

Bentley, L., A. Forner, S. Khoury, et al. 2026. "*Juniperus thurifera* Allometry Data Across a Natural Expansion Gradient in Alto Tajo, Spain" [Data set]. Zenodo. https://doi.org/10.5281/zenodo.19204141.

Binkley, D., and R. F. Fisher. 2019. *Ecology and Management of Forest Soils*. 4th ed. John Wiley & Sons.

Biodiversa+. 2022. "SPONFOREST." Biodiversa + Webside. https://www.biodiversa.eu/2022/10/31/sponforest/.

Bivand, R. S., E. Pebesma, and V. Gomez-Rubio. 2013. *Applied Spatial Data Analysis With R*. 2nd ed. Springer. https://doi.org/10.1007/978-1-4614-7618-4.

Bobbink, R., K. Hicks, J. Galloway, et al. 2010. "Global Assessment of Nitrogen Deposition Effects on Terrestrial Plant Diversity: A Synthesis." *Ecological Applications* 20, no. 1: 30–59. https://doi.org/10.1890/08-1140.1.

Camarero, J., A. Gazol, G. Sangüesa-Barreda, et al. 2018. "Forest Growth Responses to Drought at Short- and Long-Term Scales in Spain: Squeezing the Stress Memory From Tree Rings." *Frontiers in Ecology and Evolution* 6: 9. https://doi.org/10.3389/fevo.2018.00009.

Castro, J., R. Zamora, J. A. Hódar, J. M. Gómez, and L. Gómez-Aparicio. 2004. "Benefits of Using Shrubs as Nurse Plants for Reforestation in Mediterranean Mountains: A 4-Year Study." *Restoration Ecology* 12, no. 3: 352–358. https://doi.org/10.1111/j.1061-2971.2004.0316.x.

Chen, B. J. W., S. N. Teng, G. Zheng, et al. 2022. "Inferring Plant–Plant Interactions Using Remote Sensing." *Journal of Ecology* 110, no. 10: 2268–2287. https://doi.org/10.1111/1365-2745.13980.

Cook-Patton, S. C., S. M. Leavitt, D. Gibbs, et al. 2020. "Mapping Carbon Accumulation Potential From Global Natural Forest Regrowth." *Nature* 585, no. 7826: 545–550. https://doi.org/10.1038/s41586-020-2686-x.

Coomes, D. A., and P. J. Grubb. 2000. "Impacts of Root Competition in Forests and Woodlands: A Theoretical Framework and Review of Experiments." *Ecological Monographs* 70: 171–207. https://doi.org/10.1890/0012-9615.

16541103, 2026, 3, Downloaded from https://onlinelibrary.wiley.com/doi/10.1111/jvs.70142 by ALICIA FORNER - Spanish Cochrane National Provision (Ministerio de Sanidad) , Wiley Online Library on [04/05/2026]. See the Terms and Conditions (https://onlinelibrary.wiley.com/terms-and-conditions) on Wiley Online Library for rules of use; OA articles are governed by the applicable Creative Commons License

Corbane, C., K. Pipkins, S. Alleaume, et al. 2015. "Remote Sensing for Mapping Natural Habitats and Their Conservation Status—New Opportunities and Challenges." *International Journal of Applied Earth Observation and Geoinformation* 37: 7–16. https://doi.org/10.1016/J.JAG.2014.11.005.

Cramer, V. A., R. J. Hobbs, and R. J. Standish. 2007. "What's New About Old Fields? Land Abandonment and Ecosystem Assembly." *Trends in Ecology & Evolution* 23, no. 2: 104–112. https://doi.org/10.1016/j.tree.2007.10.005.

Cunningham, S. C., R. Mac Nally, P. J. Baker, et al. 2015. "Balancing the Environmental Benefits of Reforestation in Agricultural Regions." *Perspectives in Plant Ecology, Evolution and Systematics* 17: 301–317. https://doi.org/10.1016/j.ppees.2015.06.001.

Dave, R., C. Saint-Laurent, L. Murray, et al. 2018. *Second Bonn Challenge Progress Report Application of the Barometer in 2018*. IUCN. https://doi.org/10.2305/IUCN.CH.2019.06.en.

Davies, C. E., D. Moss, and M. O. Hill. 2004. *EUNIS Habitat Classification Revised 2004*. European Environment Agency.

DeSoto, L., J. M. Olano, and V. Rozas. 2016. "Secondary Growth and Carbohydrate Storage Patterns Differ Between Sexes in *Juniperus thurifera*." *Frontiers in Plant Science* 7, no. 723: 1–12. https://doi.org/10.3389/fpls.2016.00723.

DeSoto, L., J. M. Olano, V. Rozas, and M. de la Cruz. 2010. "Release of *Juniperus thurifera* Woodlands From Herbivore-Mediated Arrested Succession in Spain." *Applied Vegetation Science* 13: 15–25. https://doi.org/10.1111/j.1654-109X.2009.01045.x.

Douaihy, B., A. Maamary, R. Yammine, et al. 2022. "Forest Canopy and Mistletoe Infestation Alter the Facilitative Effects of *Juniperus oxycedrus* s.l. on Woody Seedlings on Mount Lebanon (Lebanon)." *Journal of Vegetation Science* 33, no. 6: e13163. https://doi.org/10.1111/jvs.13163.

Espelta, J. M., J. Retana, and A. Habrouk. 2003. "Resprouting Patterns After Fire and Response to Stool Cleaning of Two Coexisting Mediterranean Oaks With Contrasting Leaf Habits on Two Different Sites." *Forest Ecology and Management* 179: 401–414. https://doi.org/10.1016/S0378-1127(02)00541-8.

Europe, F. 2020. *State of Europe's Forests 2020*. Forest Europe Liaison Unit Bonn. https://foresteurope.org/state-of-europes-forests/.

European Commission. 2005. *Soil Atlas of Europe. European Soils Bureau Network*. Office for Official Publications of the European Communities.

European Environment Agency. 2019. *Updated CLC Illustrated Nomenclature Guidelines. Service Contract no 3436/R0-Copernicus/EEA.57441Task 3, D3.1—Part 1*. European Environmental Agency. https://land.copernicus.eu/user-corner/technical-library/corine-land-cover-nomenclature-guidelines/html.

Frei, T., J. M. Espelta, E. Górriz-Mifsud, et al. 2024. "Can Natural Forest Expansion Contribute to Europe's Restoration Policy Agenda? An Interdisciplinary Assessment." *Ambio* 53, no. 1: 34–45. https://doi.org/10.1007/s13280-023-01924-2.

Freschet, G. T., L. Östlund, E. Kichenin, and D. A. Wardle. 2014. "Aboveground and Belowground Legacies of Native Sami Land Use on Boreal Forest in Northern Sweden 100 Years After Abandonment." *Ecology* 95, no. 4: 963–977. https://doi.org/10.1890/13-0824.1.

Galidaki, G., D. Zianis, I. Gitas, et al. 2017. "Vegetation Biomass Estimation With Remote Sensing: Focus on Forest and Other Wooded Land Over the Mediterranean Ecosystem." *International Journal of Remote Sensing* 38, no. 7: 1940–1966. https://doi.org/10.1080/01431161.2016.1266113.

García, M., D. Riaño, E. Chuvieco, and M. Danson. 2010. "Estimating Biomass Carbon Stocks for a Mediterranean Forest in Central Spain Using LiDAR Height and Intensity Data." *Remote Sensing of Environment* 114, no. 4: 816–830. https://doi.org/10.1016/j.rse.2009.11.021.

García Morote, F. A., F. R. López Serrano, M. Andrés, E. Rubio, J. L. González Jiménez, and J. d. l. Heras. 2012. "Allometries, Biomass Stocks and Biomass Allocation in the Thermophilic Spanish Juniper Woodlands of Southern Spain." *Forest Ecology and Management* 270: 85–93. https://doi.org/10.1016/j.foreco.2012.01.007.

Gauquelin, T., V. Bertaudiere, N. Montes, W. Badri, and J. F. Asmode. 1999. "Endangered Stands of Thuriferous Juniper in the Western Mediterranean Basin: Ecological Status, Conservation and Management." *Biodiversity and Conservation* 8, no. 11: 1479–1498. https://doi.org/10.1023/A:1008966808796.

Gazol, A., J. J. Camarero, S. M. Vicente-Serrano, et al. 2018. "Forest Resilience to Drought Varies Across Biomes." *Global Change Biology* 24, no. 5: 2143–2158. https://doi.org/10.1111/gcb.14082.

Gimeno, T. E., J. J. Camarero, E. Granda, B. Pías, and F. Valladares. 2012. "Enhanced Growth of *Juniperus thurifera* Under a Warmer Climate Is Explained by a Positive Carbon Gain Under Cold and Drought." *Tree Physiology* 32, no. 3: 326–336. https://doi.org/10.1093/treephys/tps011.

Gimeno, T. E., A. Escudero, A. Delgado, and F. Valladares. 2012. "Previous Land Use Alters the Effect of Climate Change and Facilitation on Expanding Woodlands of Spanish Juniper." *Ecosystems* 15, no. 4: 564–579. https://doi.org/10.1007/s10021-012-9529-z.

Granda, E., A. Escudero, and F. Valladares. 2014. "More Than Just Drought: Complexity of Recruitment Patterns in Mediterranean Forests." *Oecologia* 176, no. 4: 997–1007. https://doi.org/10.1007/s00442-014-3064-x.

Guerrieri, R., M. Correia, I. Martín-Forés, et al. 2021. "Land-Use Legacies Influence Tree Water-Use Efficiency and Nitrogen Availability in Recently Established European Forests." *Functional Ecology* 35, no. 6: 1325–1340. https://doi.org/10.1111/1365-2435.13787.

Hampe, A., R. Alfaro-Sánchez, and I. Martín-Forés. 2020. "Establishment of Second-Growth Forests in Human Landscapes: Ecological Mechanisms and Genetic Consequences." *Annals of Forest Science* 77, no. 3: 1–5. https://doi.org/10.1007/s13595-020-00993-7.

He, X., and F. Hu. 2002. "Markov Chain Marginal Bootstrap." *Journal of the American Statistical Association* 97, no. 459: 783–795. https://doi.org/10.1198/016214502388618591.

Hegyi, F. 1974. "A Simulation Model for Managing Jack-Pine Stands." In *Growth Models for Tree and Stand Simulation*, edited by J. Fries. Royal College of Forestry.

Huang, C. Y., G. P. Asner, R. E. Martin, N. N. Barger, and J. C. Neff. 2009. "Multiscale Analysis of Tree Cover and Aboveground Carbon Stocks in Pinyon–Juniper Woodlands." *Ecological Applications* 19, no. 3: 668–681. https://doi.org/10.1890/07-2103.1.

Intergovernmental Panel on Climate Change. 2023. "Sections." In *Climate Change 2023: Synthesis Report. Contribution of Working Groups I, II and III to the Sixth Assessment Report of the Intergovernmental Panel on Climate Change*, edited by C. W. Team, H. Lee, and J. Romero, 35–115. IPCC. https://doi.org/10.59327/IPCC/AR6-9789291691647.

International Union for Conservation of Nature. 2011. "The Bonn Challenge." IUCN Website. https://www.bonnchallenge.org/.

Isenburg, M. 2014. "Rasterizing Perfect Canopy Height Models From LiDAR." Rapidlasso GmbH Website. https://rapidlasso.com/2014/11/04/rasterizing-perfect-canopy-height-models-from-lidar/%0D.

Isenburg, M. 2019. "LAStools—Efficient Tools for LiDAR Processing Version 190623." LAStools Website. http://lastools.org.

Jucker, T., J. Caspersen, J. Chave, et al. 2017. "Allometric Equations for Integrating Remote Sensing Imagery Into Forest Monitoring Programmes." *Global Change Biology* 23, no. 1: 177–190. https://doi.org/10.1111/gcb.13388.

Jung, M., P. Rowhani, T. Newbold, L. Bentley, A. Purvis, and J. P. W. Scharlemann. 2018. "Local Species Assemblages Are Influenced More

16541103, 2026, 3, Downloaded from https://onlinelibrary.wiley.com/doi/10.1111/jvs.70142 by ALICIA FORNER - Spanish Cochrane National Provision (Ministerio de Sanidad) , Wiley Online Library on [04/05/2026]. See the Terms and Conditions (https://onlinelibrary.wiley.com/terms-and-conditions) on Wiley Online Library for rules of use; OA articles are governed by the applicable Creative Commons License

by Past Than Current Dissimilarities in Photosynthetic Activity." *Ecography* 42: 670–692. https://doi.org/10.1111/ecog.04031.

Khosravipour, A., A. K. Skidmore, M. Isenburg, T. Wang, and Y. A. Hussin. 2014. "Generating Pit-Free Canopy Height Models From Airborne Lidar." *Photogrammetric Engineering & Remote Sensing* 9: 863–872. https://doi.org/10.14358/PERS.80.9.863.

Kissling, W. D., and G. Carl. 2008. "Spatial Autocorrelation and the Selection of Simultaneous Autoregressive Models." *Global Ecology and Biogeography* 17, no. 1: 59–71. https://doi.org/10.1111/j.1466-8238.2007.00334.x.

Kocherginsky, M., X. He, and Y. Mu. 2005. "Practical Confidence Intervals for Regression Quantiles." *Journal of Computational and Graphical Statistics* 14, no. 1: 41–55. https://doi.org/10.1198/106186005X27563.

Koenker, R. 2004. "Quantile Regression for Longitudinal Data." *Journal of Multivariate Analysis* 91, no. 1: 74–89. https://doi.org/10.1016/j.jmva.2004.05.006.

Koenker, R., and G. Bassett. 1982. "Tests of Linear Hypotheses and L1 Estimation." *Econometrica* 50, no. 6: 1577–1583. https://doi.org/10.2307/1913398.

Koenker, R., S. Portnoy, P. T. Ng, et al. 2019. "Quantile Regression." The R Project for Statistical Computing Website. https://www.r-project.org.

Lamb, D. 2018. "Undertaking Large-Scale Forest Restoration to Generate Ecosystem Services." *Restoration Ecology* 26, no. 4: 657–666. https://doi.org/10.1111/rec.12706.

Lasanta-Martínez, T., S. M. Vicente-Serrano, and J. M. Cuadrat-Prats. 2005. "Mountain Mediterranean Landscape Evolution Caused by the Abandonment of Traditional Primary Activities: A Study of the Spanish Central Pyrenees." *Applied Geography* 25, no. 1: 47–65. https://doi.org/10.1016/j.apgeog.2004.11.001.

Levers, C., M. Schneider, A. V. Prishchepov, S. Estel, and T. Kuemmerle. 2018. "Spatial Variation in Determinants of Agricultural Land Abandonment in Europe." *Science of the Total Environment* 644: 95–111. https://doi.org/10.1016/j.scitotenv.2018.06.326.

Lindner, M., M. Maroschek, S. Netherer, et al. 2010. "Climate Change Impacts, Adaptive Capacity, and Vulnerability of European Forest Ecosystems." *Forest Ecology and Management* 259, no. 4: 698–709. https://doi.org/10.1016/j.foreco.2009.09.023.

Malhi, Y., J. Franklin, N. Seddon, et al. 2020. "Climate Change and Ecosystems: Threats, Opportunities and Solutions." *Philosophical Transactions of the Royal Society, B: Biological Sciences* 375, no. 1794: 20190104. https://doi.org/10.1098/rstb.2019.0104.

Martín-Forés, I., C. C. Bastías, B. Acuña-Míguez, S. Magro, F. Valladares, and M. de la Cruz. 2022. "Recruitment Facilitation in Expanding Forests of Mediterranean Juniper Is Sex-Biased." *Forest Ecology and Management* 505: 119937. https://doi.org/10.1016/J.FORECO.2021.119937.

Martín-Forés, I., S. Magro, A. Bravo-Oviedo, et al. 2020. "Spontaneous Forest Regrowth in South-West Europe: Consequences for Nature's Contributions to People." *People and Nature* 2, no. 4: 980–994. https://doi.org/10.1002/pan3.10161.

Matesanz, S., and F. Valladares. 2014. "Ecological and Evolutionary Responses of Mediterranean Plants to Global Change." *Environmental and Experimental Botany* 103: 53–67. https://doi.org/10.1016/j.envexpbot.2013.09.004.

Montesinos, D., and J. Fabado. 2015. "Changes in Land Use and Physiological Transitions of a *Juniperus thurifera* Forest: From Decline to Recovery." *Canadian Journal of Forest Research* 45: 746–769. https://doi.org/10.1139/cjfr-2014-0468.

Moran, P. A. 1948. "The Interpretation of Statistical Maps." *Journal of the Royal Statistical Society. Series B, Statistical Methodology* 10, no. 2: 243–251. https://doi.org/10.1111/j.2517-6161.1948.tb00012.x.

Navarro, L. M., and H. M. Pereira. 2015. "Rewilding Abandoned Landscapes in Europe." In *Rewilding European Landscapes*, edited by H. M. Pereira and L. M. Navarro, 3–23. Springer International Publishing. https://doi.org/10.1007/s10021-012-9558-7.

NERC Airborne Research Facility. 2026. "NERC-ARF flight 2017_172 for ES17_126: Airborne Remote Sensing Measurements." NERC EDS Centre for Environmental Data Analysis, 31 March 2026. https://doi.org/10.5285/8de7d74606fe4413890a0788fb33e964.

Niinemets, Ü. 2010. "Responses of Forest Trees to Single and Multiple Environmental Stresses From Seedlings to Mature Plants: Past Stress History, Stress Interactions, Tolerance and Acclimation." *Forest Ecology and Management* 260, no. 10: 1623–1639. https://doi.org/10.1016/j.foreco.2010.07.054.

Olano, J. M., A. I. García-Cervigón, A. Arzac, and V. Rozas. 2015. "Intra-Annual Wood Density Fluctuations and Tree-Ring Width Patterns Are Sex- and Site-Dependent in the Dioecious Conifer *Juniperus thurifera* L." *Trees* 29, no. 5: 1341–1353. https://doi.org/10.1007/s00468-015-1212-5.

Olano, J. M., V. Rozas, D. Bartolomé, and D. Sanz. 2008. "Effects of Changes in Traditional Management on Height and Radial Growth Patterns in a *Juniperus thurifera* L. Woodland." *Forest Ecology and Management* 255, no. 3–4: 506–512. https://doi.org/10.1016/j.foreco.2007.09.015.

Oldén, A., A. Komonen, K. Tervonen, and P. Halme. 2016. "Grazing and Abandonment Determine Different Tree Dynamics in Wood-Pastures." *Ambio* 46: 236–277. https://doi.org/10.1007/s13280-016-0821-6.

Peña-Angulo, D., M. Khorchani, P. Errea, T. Lasanta, M. Martínez-Arnáiz, and E. Nadal-Romero. 2019. "Factors Explaining the Diversity of Land Cover in Abandoned Fields in a Mediterranean Mountain Area." *Catena* 181: 104064. https://doi.org/10.1016/j.catena.2019.05.010.

Pías, B., G. Escribano-Avila, E. Virgós, V. Sanz-Pérez, A. Escudero, and F. Valladares. 2014. "The Colonization of Abandoned Land by Spanish Juniper: Linking Biotic and Abiotic Factors at Different Spatial Scales." *Forest Ecology and Management* 329: 186–194. https://doi.org/10.1016/j.foreco.2014.06.021.

Poyatos, R., J. Latron, and P. Llorens. 2003. "Land Use and Land Cover Change After Agricultural Abandonment." *Mountain Research and Development* 23, no. 4: 362–368. https://doi.org/10.1659/0276-4741(2003)023[0362:LUALCC]2.0.CO;2.

Príncipe, A., A. Nunes, P. Pinho, L. Do Rosário, O. Correia, and C. Branquinho. 2014. "Modeling the Long-Term Natural Regeneration Potential of Woodlands in Semi-Arid Regions to Guide Restoration Efforts." *European Journal of Forest Research* 133: 757–767. https://doi.org/10.1007/s10342-014-0787-5.

R Core Team. 2021. "R: A Language and Environment for Statistical Computing." R Foundation for Statistical Computing. Vienna, Austria: R Foundation for Statistical Computing. https://www.R-project.org/.

Rodríguez-García, E., G. Gratzer, and F. Bravo. 2011. "Climatic Variability and Other Site Factor Influences on Natural Regeneration of *Pinus pinaster* Ait. In Mediterranean Forests." *Annals of Forest Science* 68: 811–823. https://doi.org/10.1007/s13595-011-0078-y.

Rouse, J. W., R. H. Haas, J. A. Schell, and D. W. Deering. 1974. "Monitoring Vegetation Systems in the Great Plains With ERTS." In Proceedings of the Third ERTS-1 Symposium, NASA Goddard Space Flight Center, 309–317. https://ntrs.nasa.gov/archive/nasa/casi.ntrs.nasa.gov/19740022614.pdf.

Rozas, V., J. M. Olano, L. DeSoto, and D. Bartolomé. 2008. "Large-Scale Structural Variation and Long-Term Growth Dynamics of *Juniperus thurifera* Trees in a Managed Woodland in Soria, Central Spain." *Annals of Forest Science* 65, no. 8: 809. https://doi.org/10.1051/forest:2008066.

Ruiz-Peinado, R., M. del Rio, and G. Montero. 2011. "New Models for Estimating the Carbon Sink Capacity of Spanish Softwood Species." *Forestry Systems* 20, no. 1: 176–188. https://doi.org/10.5424/fs/2011201-11643.

16541103, 2026, 3, Downloaded from https://onlinelibrary.wiley.com/doi/10.1111/jvs.70142 by ALICIA FORNER - Spanish Cochrane National Provision (Ministerio de Sanidad) , Wiley Online Library on [04/05/2026]. See the Terms and Conditions (https://onlinelibrary.wiley.com/terms-and-conditions) on Wiley Online Library for rules of use; OA articles are governed by the applicable Creative Commons License

Sato, C. F., D. Florance, and D. B. Lindenmayer. 2019. "Drivers of Temperate Woodland Condition Through Time in an Agricultural Landscape." *Land Degradation and Development* 30, no. 11: 1357–1367. https://doi.org/10.1002/ldr.3325.

Sato, C. F., J. T. Wood, J. A. Stein, et al. 2016. "Natural Tree Regeneration in Agricultural Landscapes: The Implications of Intensification." *Agriculture, Ecosystems and Environment* 230: 98–104. https://doi.org/10.1016/j.agee.2016.05.036.

Schenk, H. J., and R. B. Jackson. 2002. "Rooting Depths, Lateral Root Spreads and Belowground Aboveground Allometries of Plants in Water Limited Ecosystems." *Journal of Ecology* 90: 480–494. https://doi.org/10.1046/j.1365-2745.2002.00682.x.

Schmidt, G., C. Jenkerson, J. Masek, E. Vermote, and F. Gao. 2013. "Landsat Ecosystem Disturbance Adaptive Processing System (LEDAPS) Algorithm Description." U.S. Geological Survey Open-File Report 2013–1057. https://doi.org/10.3133/ofr20131057.

Seddon, N., A. Chausson, P. Berry, C. A. J. Girardin, A. Smith, and B. Turner. 2020. "Understanding the Value and Limits of Nature-Based Solutions to Climate Change and Other Global Challenges." *Philosophical Transactions of the Royal Society, B: Biological Sciences* 375: 20190120. https://doi.org/10.1098/rstb.2019.0120.

Shoshany, M. 2000. "Satellite Remote Sensing of Natural Mediterranean Vegetation: A Review Within an Ecological Context." *Progress in Physical Geography: Earth and Environment* 24, no. 2: 153–178. https://doi.org/10.1177/030913330002400201.

Simonson, W., P. Ruiz-Benito, F. Valladares, and D. Coomes. 2015. "Modelling Above-Ground Carbon Dynamics Using Multi-Temporal Airborne Lidar: Insights From a Mediterranean Woodland." *Biogeosciences Discussions* 12, no. 17: 14739–14772. https://doi.org/10.5194/bgd-12-14739-2015.

Smit, C., J. Den Ouden, and M. Díaz. 2008. "Facilitation of *Quercus ilex* Recruitment by Shrubs in Mediterranean Open Woodlands." *Journal of Vegetation Science* 19, no. 2: 193–200. https://doi.org/10.3170/2007-8-18352.

Tian, L., X. Wu, Y. Tao, et al. 2023. "Review of Remote Sensing-Based Methods for Forest Aboveground Biomass Estimation: Progress, Challenges, and Prospects." *Forests* 14, no. 6: 1086. https://doi.org/10.3390/f14061086.

United Nations General Assembly. 2015. *Transforming Our World: The 2030 Agenda for Sustainable Development*. United Nations.

Vayreda, J., J. Martinez-Vilalta, M. Gracia, J. G. Canadell, and J. Retana. 2016. "Anthropogenic-Driven Rapid Shifts in Tree Distribution Lead to Increased Dominance of Broadleaf Species." *Global Change Biology* 22, no. 12: 3984–3995. https://doi.org/10.1111/gcb.13394.

Vilà-Cabrera, A., J. M. Espelta, J. Vayreda, and J. Pino. 2017. "'New Forests' From the Twentieth Century Are a Relevant Contribution for C Storage in the Iberian Peninsula." *Ecosystems* 20: 130–143. https://doi.org/10.1007/s10021-016-0019-6.

Villellas, J., I. Martín-Forés, S. Mariette, et al. 2020. "Functional Distance Is Driven More Strongly by Environmental Factors Than by Genetic Relatedness in *Juniperus thurifera* L. Expanding Forest Stands." *Annals of Forest Science* 77, no. 3: 1–18. https://doi.org/10.1007/S13595-020-00973.

Weissteiner, C. J., M. Boschetti, K. Böttcher, P. Carrara, G. Bordogna, and P. A. Brivio. 2011. "Spatial Explicit Assessment of Rural Land Abandonment in the Mediterranean Area." *Global and Planetary Change* 79, no. 1–2: 20–36. https://doi.org/10.1016/j.gloplacha.2011.07.009.

Yüksel, A., A. Akay, and R. Gundogan. 2008. "Using ASTER Imagery in Land Use/Cover Classification of Eastern Mediterranean Landscapes According to CORINE Land Cover Project." *Sensors* 8, no. 2: 1237–1251. https://doi.org/10.3390/s8021287.

Supporting Information

Additional supporting information can be found online in the Supporting Information section. **Appendix S1:** Land cover classification and link with topography. **Appendix S2:** Data at the tree level. **Appendix S3:** Mapping juniper growth at the landscape level. **Appendix S4:** Juniper growth at the individual scale and effects of sex and intraspecific competition. **Appendix S5:** Effect of topography and interspecific competition on juniper growth at the landscape scale.

16541103, 2026, 3, Downloaded from https://onlinelibrary.wiley.com/doi/10.1111/jvs.70142 by ALICIA FORNER - Spanish Cochrane National Provision (Ministerio de Sanidad) , Wiley Online Library on [04/05/2026]. See the Terms and Conditions (https://onlinelibrary.wiley.com/terms-and-conditions) on Wiley Online Library for rules of use; OA articles are governed by the applicable Creative Commons License

Supporting information to the paper

Bentley L., A. Forner, S. Khoury, F. Valladares, D.A. Coomes, and I. Martín-Forés. Turning Mediterranean farmlands into priority habitats: Natural expansion of juniper woodlands after agricultural abandonment. *Journal of Vegetation Science*.

Appendix S1. Land cover classification and link with topography.

S1.1. Land cover classification, training points and protocol

The four land cover classes in which we classified our study landscape are described in Table S1.1.1.

Table S1.1.1 Classes used in the training and classification of land cover and its consumers' and producers' accuracy in the region of Alto Tajo Natural Park. The number of train points used per modal class is shown, along with the number of training point years per class in brackets.

Land cover class	Definition	Training points	Validation points	Consumer's Accuracy	Producer's Accuracy
Agriculture	Arable land with signs of cultivation and possible irrigation.	29 (48)	14 (19)	78.6	57.9
Grassland and dwarf shrubland	Open areas dominated by short vegetation, (5-50 cm tall), with no evidence of cultivation or irrigation and less than 10 % tree cover.	86 (433)	37 (48)	55.9	68.8
Woodland and shrubland	A relative tree or shrub cover of greater than 20 %, but less than 80 %. Individuals are > 0.5 m tall and may reach up to 10 m.	120 (212)	50 (81)	78.5	76.5
Closed forest	Trees over 5 m tall with attached canopies; in the region evergreen, deciduous and mixed forests.	50 (92)	23 (40)	91.7	82.5

Landsat images used to classify landscape into four cover classes for 17 years (1984-2018) were thoroughly checked to identify clouds. To avoid cloud effects on data quality, we only considered extracted Landsat data (from six Landsat bands, Table S1.1.2) when cloud cover was lower than 20 %. Moreover, we masked any remaining clouds and cloud shadows prior to the formation of image composites using masks obtained from image metadata, provided by the United States Geological Survey (USGS). The abundance of cloud cover in some years and the presence of scenes with visible artefacts, which were also excluded from subsequent processing, meant that composite scenes were not assembled for every year. When composites in one year did not cover the entire area of interest (this only happened in three cases) we combined the summer and winter images of adjacent years to produce a complete image. The year of the imagery contributing most of the coverage was recorded as the year of the composite.

Table S1.1.2. Wavelengths (μm) of Landsat bands used in the training and prediction of land cover from 1984-2018.

Satellite	Blue	Green	Red	Near Infrared	Shortwave Infrared 1	Shortwave Infrared 2
Landsat 5	0.45-0.52	0.52-0.60	0.63-0.69	0.77-0.90	1.55-1.75	2.08-2.35
Landsat 7	0.45-0.52	0.52-0.60	0.63-0.69	0.77-0.90	1.55-1.75	2.08-2.35
Landsat 8	0.45-0.51	0.53-0.59	0.64-0.67	0.85-0.88	1.57-1.65	2.11-2.29

Each manual classification point generated was classified as one of the focal land classes (Table S1.1.1), based on a 30m buffer surrounding each point. Each point was assigned a landcover for each year in which satellite data was available on *Google Earth Pro* (30-50 cm resolution, acquired by CNES/AIRBUS). For each location, a 30 m buffer was used to define the areas around each point was us, and if the point was on the side of a road, we double checked our classification by using *Google Street View* imagery corresponding to a year for which *Google Earth* data was available. Therefore, we classified each point based on the 30 m² surrounding it and repeated this for multiple years (2004-2018) to account for interannual variation (Table S1.1.3), which resulted in 673 classifications of 409 spatially unique points. Due to incomplete satellite image coverage and cloud cover, 3 % of the points remained unclassified. Where we found pixels with mixed classes, we recorded the class that occupied most of the land cover. We manually masked all urban areas from land cover classification and subsequent analyses due to their low coverage and lack of training data.

Table S1.1.3. Years in which training, and validation point-years were trained or validated, using satellite and street view imagery from *Google Earth Pro.*

Year	Training points	Validation Points
2004	9	3
2009	48	21
2010	50	18
2011	112	42
2014	9	2
2015	209	81
2017	1	0
2018	47	21

Due to uncertainty in the quality of georeferencing in the satellite imagery provided by *Google Earth Pro*, the locations of all training and validation points were cross checked against robustly georeferenced 2019 satellite imagery also acquired by CNES/AIRBUS, but accessible via the basemap of *Google Earth Engine*. A high degree of accuracy was found for all points, with over 90 % showing less than 1 m of displacement. Where an offset in satellite imagery was found, it was commonly less than 3 m and would have had no impact on point classification. However, where an offset was observed, the classification was based on the 30 m surrounding the true location of the point, as shown by *Google Earth Engine*.

Regarding the training of the model, we ensured all multi-year classifications for a given point were included in the same data subset to avoid inflating the validation score and therefore, the accuracy. To ensure the difference in Landsat bandwidths between Landsat 8 and 7 did not impact on the classifier, we performed a second hindcasting validation, by using training points from 2014-2018 against points from 2004-2013, achieving a cross-validation accuracy of 71.4 %.

Due to the scarcity of urban areas in the region, insufficient reference points were available to reliably identify these areas. Therefore, we removed reference points classified as urban (26 points) and masked urban areas in all data sets used to inform the land cover classifier using the 2018 CORINE land cover data, prior to classifying other land cover classes. The final reference data set consisted of 409 points (spatially unique) and 673 point-years (including multi-year classifications). The Random Forest classifier was trained over 300 trees with a bag fraction of 0.7 and a minimum leaf population of 3. Manual validation data points were matched to the corresponding sites in the relevant year. We calculated the overall cross validation accuracy and the producers and consumers accuracy for the identification of each land cover class individually.

S1.2. Calculation of topography elements

To identify links between land cover change over time and topography we obtained data on elevation (m), slope (degrees), and annual solar insolation ($kW.m^{-2}.year^{-1}$).

Elevation and slope were extracted from the structure-from-motion derived from Digital Terrain Model (DTM) and aggregated to the resolution of land cover maps.

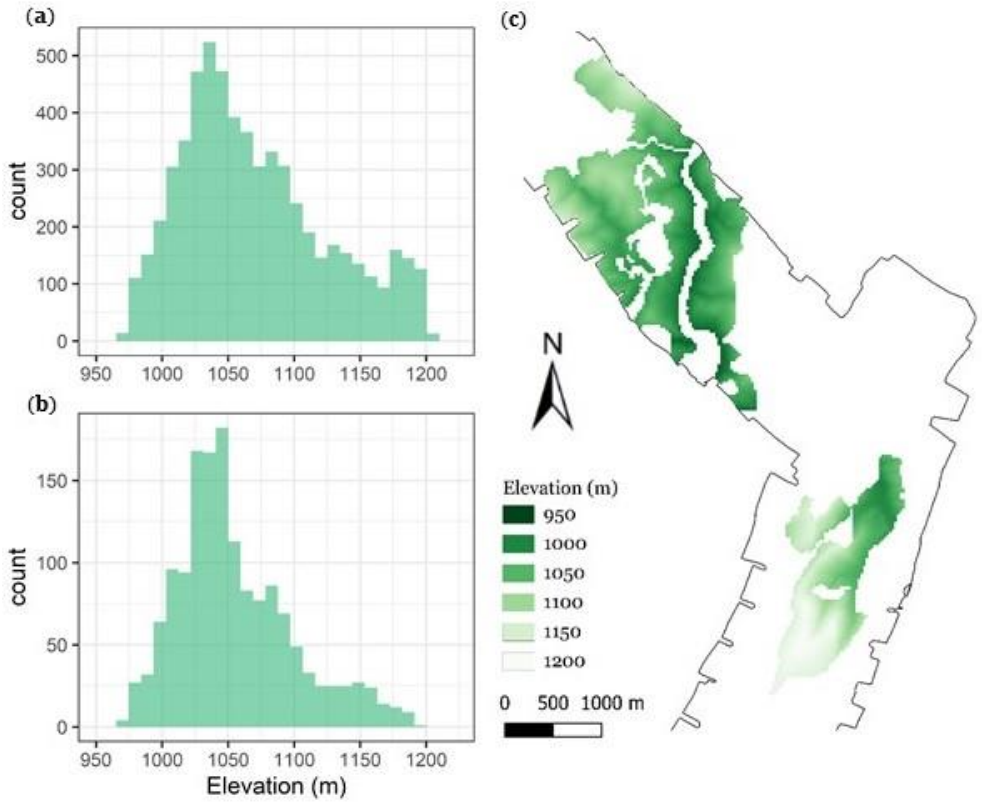

Figure S1.2.1. Distribution of elevation values across the area confirmed to be monospecific *Juniperus thurifera* in the field. (**a**) Elevations of the areas identified as juniper; (**b**) Elevations of the 1500 pixels used in the analysis of variation in above ground biomass (see main text); (**c**) Spatial distribution of elevation values in the area confirmed to be monospecific *J. thurifera* in the field.

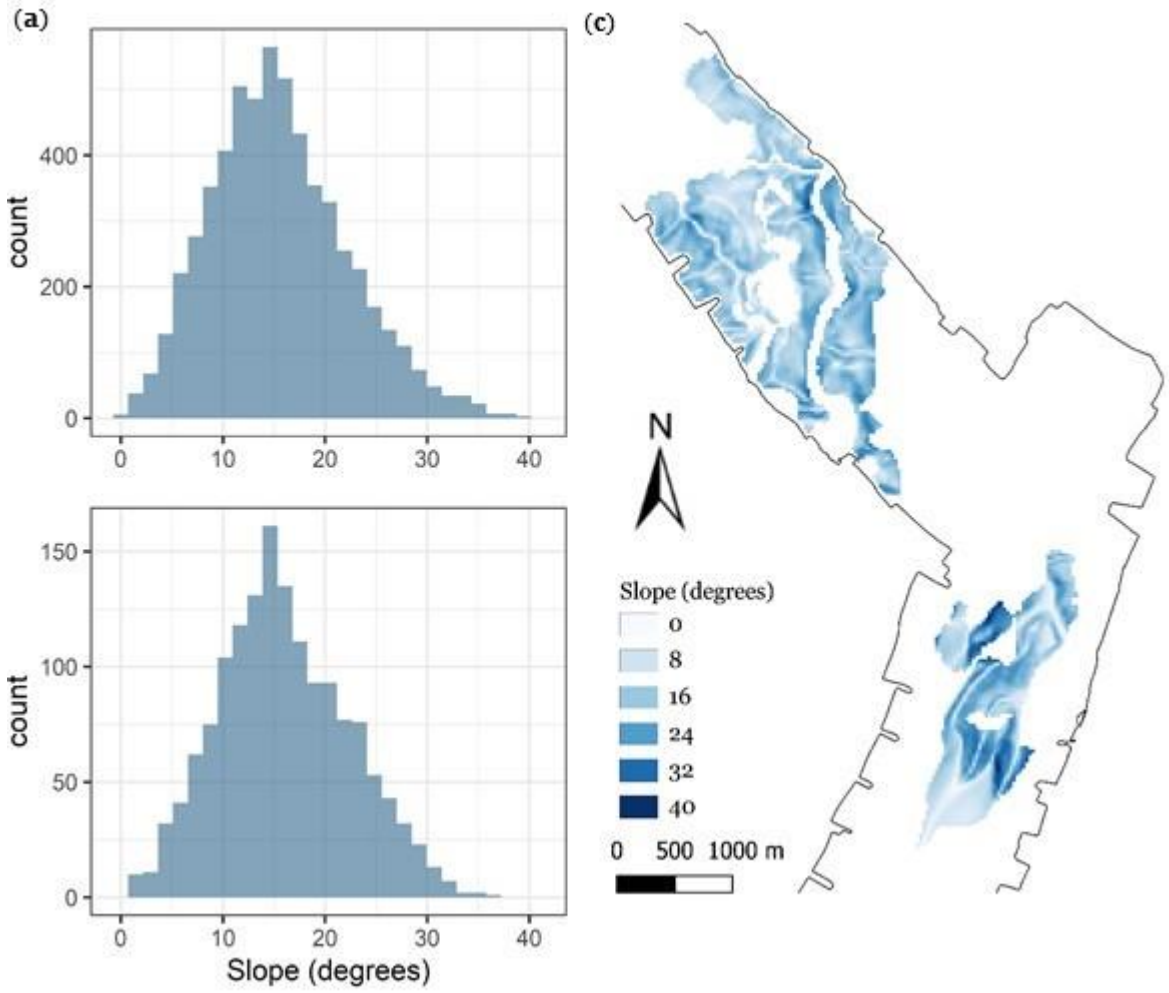

Figure S1.2.2. Distribution of slope values across the area confirmed to be monospecific *J. thurifera* in the field. (**a**) Slope of the areas identified to be juniper; (**b**) Slopes of the 1500 pixels used in the analysis of variation in above ground biomass (see main text); (**c**) Spatial distribution of slope values in the area confirmed to be monospecific *J. thurifera* in the field.

Solar insolation was calculated at a 5 m resolution using a digital terrain model, slope map and aspect map calculated from the Spanish national DTM at a 5 m resolution (MDT05 2009 CC-BY 4.0, Instituto Geográfico Nacional, 2009), produced by the National Geographic Institute of Spain and the autonomous communities of Catalonia, Castilla La Mancha, Galicia, Region of Murcia and Valencian Community. All analyses were performed in Grass GIS 7.8 (GRASS Development Team, 2019) using the *r.sun.daily* addon (Petras and Petrasova 2019). This source enables the use of a 0.1-degree buffer around the study area during the calculation of insolation, to account for topographic shadows cast from outside the area of interest.

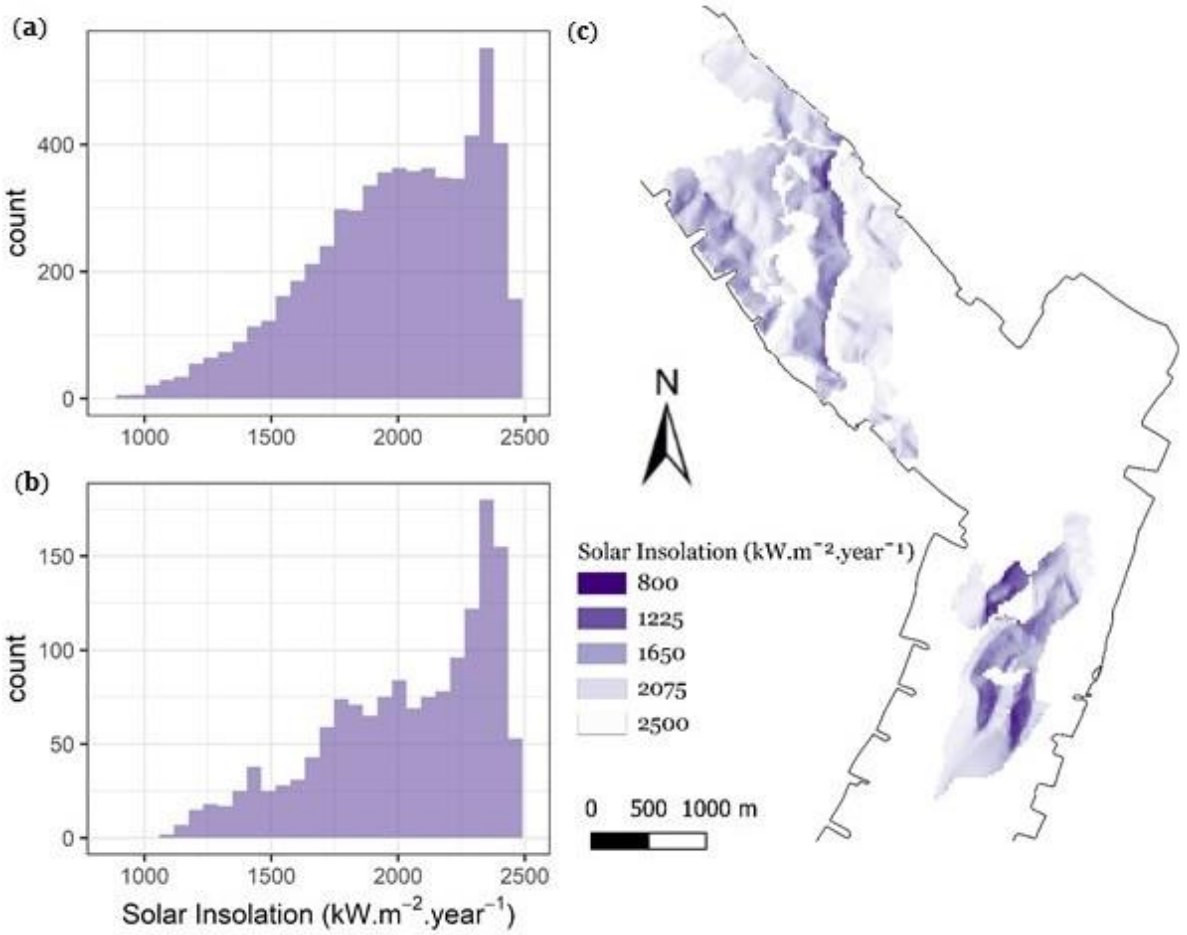

Figure S1.2.3. Distribution of solar insolation values across the area confirmed to be monospecific *J. thurifera* in the field. (**a**) Insolation of the area identified to be juniper; (**b**) Insolation of the 1500 pixels used in the analysis of variation in above ground biomass (see main text); (**c**) Spatial distribution of insolation values in the area confirmed to be monospecific *J. thurifera* in the field.

Horizon angle height was calculated using r.horizon (Huld et al. 2007) for all aspects at 45-degree intervals and subsequently used in the calculation of annual insolation via the addon r.sun.daily (Petras and Petrasova 2019). Albedo was calculated from a composite of values for black-sky albedo for the visible spectrum, via Google Earth Engine (2000-2019) after all data without full Bidirectional Reflectance Distribution Function (BRDF) inversions were masked (Schaaf and Wang 2015). Linke turbidity coefficient was calculated from 10 random values extracted for the study area from the Linke turbidity factor data set of the SoDa project (Remund et al. 2003). Calculated landscape albedo was 0.21 and the Linke turbidity coefficient was 0.337 (SD = 0.067). Solar insolation (data accessed from www.soda-pro.com) was aggregated to a 26.9 m resolution. A 0.1-degree buffer was employed around the study site for all calculations. Solar insolation was calculated for even hours in a 24-hour period, for 365 days of the year. Annual insolation was calculated as the sum of daily solar insolation over a 365-day period.

S1.3. Land cover distribution linked with topography

Rates of change in elevation, slope and solar insolation are provided in Tables S1.3.1 and S1.3.2. Moreover, those rates are shown for each quantile and each land cover classification used in the quantile regressions. Those calculations were used to assess how land cover patterns had changed with respect to topography, over the 34 years of study. Consumer and producer's accuracies were both highest for open woodland and closed forest. The challenge of distinguishing between unirrigated arable agriculture and grassland resulted in a lower consumer and producer's accuracy for those classes.

Table S1.3.1. Rate of change (with standard errors) in land cover area ($km^2.year^{-1}$) in a depopulated region of central Spain, along with standard error estimates, for 1984-2018. The absolute area and median elevation (m), slope (degrees) and solar insolation ($kW.m^{-2}.year^{-1}$) for each land cover class, at the beginning and end of the studied time series, are also shown, with the interquartile ranges for elevation, slope and solar insolation.

Land cover class	**Elevation**		**Slope**		**Solar insolation**	
Year	**1984**	**2018**	**1984**	**2018**	**1984**	**2018**
Agriculture	1130 ± 111	1132 ± 109	7.73 ± 8.13	5.22 ± 5.69	2072 ± 213	2078 ± 162
Grassland and dwarf shrubland	1095 ± 115	1133 ± 112	14.48 ± 11.68	10.47 ± 11.64	2061 ± 340	2050 ± 255
Woodland and shrubland	1091 ± 112	1078 ± 110	21.55 ± 13.78	15.31 ± 12.53	2157 ± 692	2114 ± 438
Closed forest	1108 ± 32	1095 ± 72	30.20 ± 15.06	21.23 ± 7.94	2099 ± 644	2131 ± 431

Table S1.3.2. Rates of change in land cover elevation (m.year^{-1}), slope (degrees.year^{-1}) and solar insolation (kW.m^{-2}.year^{-2}), for each quantile used in quantile regression, along with standard error estimates for the rates of change for 1984-2018, in the region of study in central Spain. Median elevation, slope and insolation are provided for each land cover class at the beginning and end of the studied time series, along with the relevant interquartile ranges. All slopes are significant at the $P < 0.0001$ level, except for slopes marked † which were not significant, and ‡ which were significant at the $P < 0.05$ level.

Land cover Class	**Change in elevation per quantile**					**Quantile significance**	
	10	**25**	**50**	**75**	**90**	**F**	***P***
Agriculture	0.23 ± 0.03	-0.09 ± 0.02	-0.15 ± 0.03	-0.11 ± 0.02	-0.22 ± 0.02	46.8	<0.0001
Grassland and dwarf shrubland	0.40 ± 0.02	0.89 ± 0.02	0.85 ± 0.02	0.57 ± 0.02	0.27 ± 0.01	280.9	<0.0001
Woodland and Shrubland	-0.01 ± 0.02 †	-0.05 ± 0.02 ‡	-0.12 ± 0.03	-0.09 ± 0.03 ‡	0.05 ± 0.02 ‡	11.0	<0.0001
Closed Forest	0.01 ± 0.04 †	-0.05 ± 0.17 †	-0.01 ± 0.08 ‡	0.35 ± 0.06	0.39 ± 0.10	15.0	<0.0001
	Change in slope per quantile						
Agriculture	-0.011 ± 0.001	-0.030 ± 0.002	-0.065 ± 0.002	-0.109 ± 0.003	-0.146 ± 0.005	278.2	<0.0001
Grassland and Dwarf shrubland	-0.027 ± 0.002	-0.040 ± 0.002	-0.069 ± 0.002	-0.065 ± 0.002	-0.041 ± 0.004	99.2	<0.0001
Woodland and Shrubland	-0.036 ± 0.003	-0.066 ± 0.003	-0.108 ± 0.003	-0.083 ± 0.003	-0.051 ± 0.004	115.9	<0.0001
Closed Forest	-0.033 ± 0.018 †	-0.056 ± 0.013	-0.087 ± 0.017	-0.117 ± 0.017	-0.278 ± 0.021	13.7	<0.0001
	Change in solar insolation per quantile						
Agriculture	5.19 ± 0.21	2.24 ± 0.08	0.83 ± 0.06	0.42 ± 0.05	-0.07± 0.07 †	204.4	<0.0001
Grassland and dwarf shrubland	0.89 ± 0.13	0.33 ± 0.07	-0.50 ± 0.05	-1.16 ± 0.04	-1.66 ± 0.05	146.7	<0.0001
Woodland and Shrubland	3.58 ± 0.17	2.45 ± 0.21	-1.31 ± 0.12	-1.55 ± 0.07	-1.00 ± 0.05	241.1	<0.0001
Closed Forest	-10.30 ± 1.52	-5.45 ± 0.55	-6.01 ± 0.43	-1.45 ± 0.26	-0.72± 0.22	47.4	<0.0001

References

GRASS Development Team. 2019. “Geographic Resources Analysis Support System (GRASS) Software, Version 7.8.” Open Source Geospatial Foundation. Accessed 2020. https://grass.osgeo.org/

Huld, T., T. Cebecauer, J. Hofierka, and M. Suri. 2007. “r.horizon: Horizon Angle Computation Module.” In Geographic Resources Analysis Support System (GRASS GIS) Software, Version 7.8. Open Source Geospatial Foundation. Accessed 2020. https://grass.osgeo.org/grass-stable/manuals/r.horizon.html

Petras, V., and A. Petrasova. 2019. “r.sun.daily: Daily Solar Irradiance and Geometry Module.” In Geographic Resources Analysis Support System (GRASS GIS) Software, Version 7.8. Open Source Geospatial Foundation. Accessed 2020. https://grass.osgeo.org/grass-stable/manuals/addons/r.sun.daily.htmlr

Remund, J., L. Wald, M. Lefèvre, T. Ranchin, and J. Page. 2003. “Worldwide Linke turbidity information.” In Proceedings of the ISES Solar World Congress, 16-19 June 2003, Göteborg, Sweden.

Schaaf, C., and Z. Wang, Z. 2015. “MCD43A3 MODIS/Terra+Aqua BRDF/Albedo Daily L3 Global - 500 m V006.” [Data set]. NASA EOSDIS Land Processes DAAC. https://doi.org/https://doi.org/10.5067/MODIS/MCD43A3.006.

Supporting information to the paper

Bentley L., A. Forner, S. Khoury, F. Valladares, D.A. Coomes, and I. Martín-Forés. Turning Mediterranean farmlands into priority habitats: Natural expansion of juniper woodlands after agricultural abandonment. *Journal of Vegetation Science*.

Appendix S2. Data at the tree level.

S2.1. Field-measurements at the tree level

We used Geneq iSXBlueII+ GNSS Receiver RTK as the differential geographic positioning system to georeferenced individual trees in the field. We measured tree height with a Haglof Vertex IV hypsometer, and we used a DME-distance measurer (Haglöf, Sweden) to measure the two perpendicular axes centred on the trunk to calculate crown diameter.

To calculate tree age, we bored the trees at a height of 50 cm using a Pressler increment borer to extract wood cores with intact pith extending the trunk diameter. We air-dried the cores, glued them onto wooden mounts, and polished them with progressively finer sandpaper until the tree rings became visible. We then estimated the age for each tree by examining the cores with a stereomicroscope. We scanned the tree rings at 2400 dpi and measured ring widths with CooRecorder v9.3 (Cybis Elektronik, 2018) to an accuracy of 0.001 mm. We checked cross-dating using CooRecorder v9.3 and COFECHA 169 (Holmes, 1983).

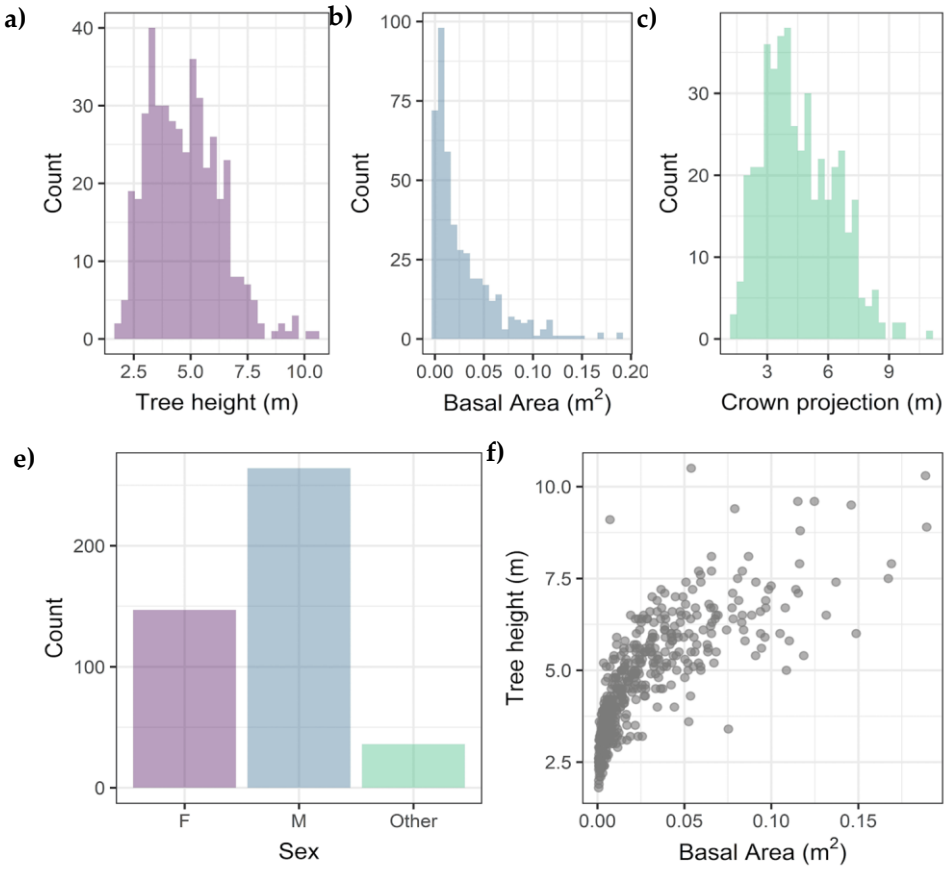

Figure S2.1.1. Graphical summary of the properties of the individual J. thurifera surveyed from 2017-2019 across 10 plots in Alto Tajo Natural Park, Spain for (a) tree height, (b) basal area, (c) crown projection (m), (d) sex and (e) the relationship between tree height and basal area for 447 individuals.

S2.2. Tree level allometry data and statistics

The allometry used is shown in equations (Eq. S2.2.1-S2.2.5), where d is quadratic mean stem diameter (m) and h is tree height (m). This allometry was developed using individuals from Alto Tajo Natural Park and has been previously validated against remote sensing estimates for this region (Ruiz-Peinado et al. 2011; Simonson et al. 2015).

$$Biomass_j = B_{j\,Stem} + B_{j\,Branc\,L} + B_{j\,Branc\,M} + B_{j\,Branc\,S\,and\,Needles} \quad \text{(Eq. S2.2.1)}$$

$$B_{j\,Stem} = 0.0132 \times d_j^2 \times h_j + 0.217 \times d_j \times h_j \quad \text{(Eq. S2.2.2)}$$

$$B_{j\,Branc\,L} = \left[0.107 \times \left(d_j - 22.5\right)^2\right] \times Z \quad \text{where } Z = \begin{cases} 0\ if\ d_j \leq 22.5 \\ 1\ if\ d_j > 22.5 \end{cases} \quad \text{(Eq. S2.2.3)}$$

$$B_{j\,Branc\,M} = 0.00792 \times d_j^2 \times h \quad \text{(Eq. S2.2.4)}$$

$$B_{j\,Branc\,S\,and\,Needles} = 0.273 \times d_j \times h_j \quad \text{(Eq. S2.2.5)}$$

Information regarding the distribution of individual allometric traits for the *J. thurifera* located on our plots is presented in Figure S2.1.1. The data provided shows the distribution of traits used in analyses, but not otherwise depicted, including tree heights, basal area, crown projection, and sex.

S2.3. Aggregating tree level measurements at the plot level

We aggregated the data obtained at the tree level to estimate biomass, tree density and sex ration per plot in each of the stages of the gradient of forest expansion. Table S2.3.1 shows the tree-level and plot-level properties.

Table S2.3.1. Summary of the average tree characteristics (height (m), tree quadratic diameter (QD) as estimated from stem diameter at breast height (dbh) (cm) as $QD = \sqrt{\sum dbh_{1-n}^2}$ where n is the number of stems, basal area (m^2), age (years) and biomass ($kg.tree^{-1}$)) and plot characteristics (biomass ($Mg.ha^{-1}$), tree density per plot ($trees.ha^{-1}$) and sex ratio (male:female)) with standard error for each regeneration stage (expansive front, transition zone and mature forest). Individuals that were hermaphrodite or not clearly identifiable as either male or female were excluded in the calculation of the sex ratio for each plot. Notice that biomass refers only to above-ground biomass.

		Tree-level properties					**Plot-level properties**		
Stage	**Number of plots**	**Height**	**QD**	**Basal area**	**Age**	**Biomass**	**Biomass**	**Density**	**Sex ratio**
Expansion front	4	4.08 ± 0.11	12.4 ± 0.6	0.016 ± 0.002	22.8 ± 0.9	52.3 ± 5.3	1.8 ± 0.4	36.9 ± 10.7	2.2 ± 0.3
Transition zone	3	4.75 ± 0.12	16.8 ± 0.8	0.029 ± 0.003	25.0 ± 1.3	93.3 ± 8.3	12.4 ± 7.4	0.8 ± 0.5	1.8 ± 0.3
Mature forest	3	5.33 ± 0.13	19.7 ± 0.9	0.040 ± 0.003	39.0 ± 1.6	133.5 ± 11.6	16.8 ± 3.2	126.2 ± 25.0	1.7 ± 0.2

References

Holmes, R. L. 1983. “Computer-assisted quality control in tree-ring dating and measurement.” Tree-Ring Bulletin 43: 69–78.

Ruiz-Peinado, R., M. del Rio, and G. Montero. 2011. “New models for estimating the carbon sink capacity of Spanish softwood species.” Forest Systems 20(1): 176–188. https://doi.org/10.5424/fs/2011201-11643

Simonson, W., P. Ruiz-Benito, F. Valladares, and D. Coomes. 2015. “Modelling above-ground carbon dynamics using multi-temporal airborne LIDAR: insights from a Mediterranean woodland.” Biogeosciences Discussions 12(17): 14739–14772. https://doi.org/10.5194/bgd-12-14739-2015

Supporting information to the paper

Bentley L., A. Forner, S. Khoury, F. Valladares, D.A. Coomes, and I. Martín-Forés. Turning Mediterranean farmlands into priority habitats: Natural expansion of juniper woodlands after agricultural abandonment. *Journal of Vegetation Science*.

Appendix S3. Mapping juniper growth at the landscape level.

S3.1. Airborne data collection

The Dornier 228 aircraft was carrying an iXU-RS1000 (50 mm) camera at an altitude of 1.13 km, on 19th June 2017, and collected Red Green Blue (RGB) images at a resolution of 9.48 cm.pixel^{-1}. Aerial imagery was georeferenced using a Leica global navigation satellite system base station located at Huertahernando, provided by the Natural Environment Research Council (NERC) Geophysical Equipment Facility (n.d.). A further 21 georeferenced points were collected across the landscape to facilitate subsequent orthorectification. Digital imagery collected by the NERC Airborne Research and Survey Facility (NERC-ARF) was orthorectified (Figure 1(a) in the main text) and processed using Agisoft Photoscan v1.4.0 build 5650 by NERC-ARF Data Analysis Node (DAN) to produce a structure-from-motion (SFM) derived point cloud containing over 160,000,000 points with an average point density of 8.42 m^{-2} and an estimated error of 0.24 m in longitude and latitude and of 0.58 m in altitude.

A summary of the survey data collected by the NERC-ARF project ES17/126 on 19th June 2017 is provided, along with details of the processing carried out by NERC-ARF-DAN to produce the orthomosaic and dense point cloud (Figure S3.1 and Table S3.1). Areas associated with 2 or fewer viewing angles were excluded from the landscape biomass analyses. All graphics and data in S3 were provided by NERC-ARF-DAN.

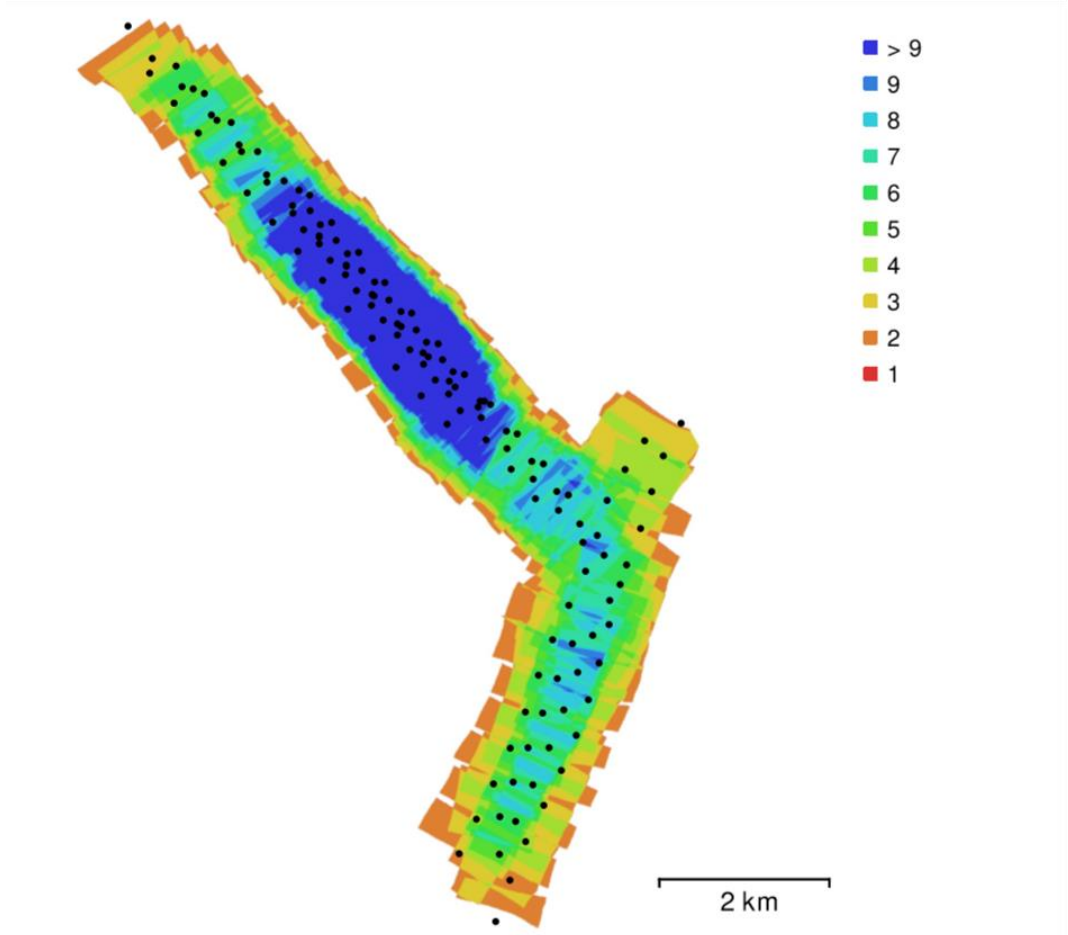

Figure S3.1. Camera locations (points) and image overlap of remote survey data processed via Agisoft Photoscan to assemble an orthomosaic and dense point cloud produced by NERC-ARF-DAN.

Table S3.1. Summary of the RGB data collected by NER-ARF on 19th June 2017 and subsequent processing parameters.

Data Properties		**Dense Point Cloud Reconstruction Parameters**	
Number of Images	142	Points	162,953,704
Camera Stations	137	Quality	Medium
Flight altitude (km)	1.13	Depth Filtering	Aggressive
Ground Resolution (cm.pixel^{-1})	9.48		
Reprojection error (pixel)	0.376		
Coverage area (km^2)	19.6		
Control points	21		
Point Cloud Alignment Parameters		**Orthomosaic Reconstruction Parameters**	
Accuracy	Highest	Blending mode	Mosaic
Generic preselection	Yes	Enable hole filling	Yes
Reference preselection	Yes	Surface	DEM
Key point limit	40,000		
Tie point limit	4,000		
Adaptive camera	Yes		

S3.2. Scaling plot biomass estimates to the landscape scale

We compared models of biomass as a function of either top of canopy height, canopy fraction or the interaction between the two and carried out a leave-one-out regression on log transformed data of the biomass at the plot level ($Biomass_{Plot}$). This enabled a linear analysis satisfying normality. We selected the model with the lowest percentage bias (Eq. S3.2.1), root mean squared error (RMSE) and mean absolute error (MAE) to predict landscape biomass. Percentage bias was calculated as equation (Eq. S3.2.2), RMSE was calculated as equation (Eq. S3.2.3) and MAE was calculated as equation (Eq. S3.2.4), where O_i is an observed value in an independent validation data set, P_i is the predicted value for the observed data point and n is the number of validation data points.

$$Percentage\ bias = \frac{100}{n} \times \Sigma\ \frac{P_i - O_i}{O_i} \quad \text{(Eq. S3.2.1)}$$

$$RMSE = \sqrt{\frac{1}{n}\Sigma(P_i - O_i)^2} \quad \text{(Eq. S3.2.2)}$$

$$MAE = \frac{1}{n}\Sigma(P_i - O_i) \quad \text{(Eq. S3.2.3)}$$

To account for error introduced by the anti-logarithmic conversion, a correction factor (C) was calculated using equation (Eq. S3.2.5) where SEE is the standard error of estimation, calculated as equation (Eq. S3.2.6), where *n* is the sample size and O_i and P_i are observed and predicted values used in the leave-one-out regression cross validation (Baskerville, 1972).

$$C = exp(\frac{SEE^2}{2}) \quad \text{(Eq. S3.2.4)}$$

$$SEE = \sqrt{\Sigma\frac{(O_i - P_i)^2}{n}} \quad \text{(Eq. S3.2.5)}$$

The relationship between predicted values of biomass at the landscape level derived from SFM ($Biomass_{SFM}$) and allometry based values of $Biomass_{Plot}$ was defined by the equation S3.2.6. and is shown in Figure S3.2.1. There was a positive correlation between plot canopy fraction and top of canopy height within the calibration data set (Pearson's r = 0.774; P < 0.01), indicating lower canopy fractions and shorter trees at the expanding front of juniper woodlands. The landscape biomass distribution is shown in Figure S3.2.2.

$$Biomass_{SFM} = 32.9 \text{ x } 1.11(Top\ of\ canopy\ height\ x\ canopy\ fraction)^{0.62} \quad \text{(Eq. S3.2.6)}$$

The best-fit biomass model of $Biomass_{SFM}$ allowed us to generalise our estimates of biomass to the landscape scale, comprising a wider range of conditions than those it is practical to collect field data for. $Biomass_{SFM}$ was estimated at the resolution of Landsat imagery (26.9 m^2) over an area of 4.3 km. As this resolution was smaller than the mean plot size (94.7 m^2), we also calculated $Biomass_{SFM}$ at a resolution of 80.6 m and 107.5 m, and estimated the percentage bias, RMSE and MAE introduced by variation in resolution, to ensure resolution did not bias model results.

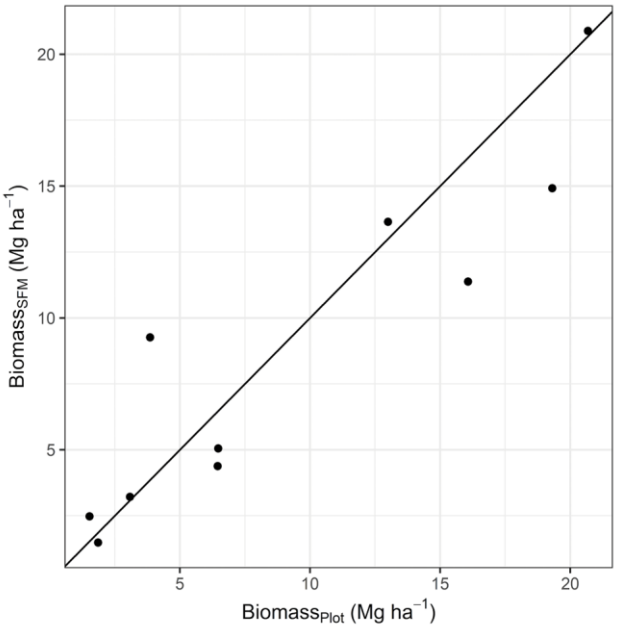

Figure S3.2.1. Plot above ground biomass ($Biomass_{Plot}$) estimates compared to the remote sensing derived estimates of Biomass ($Biomass_{SFM}$) produced by leave-one-out regression of $Biomass_{Plot}$ as a function of mean top of canopy height and canopy cover fraction.

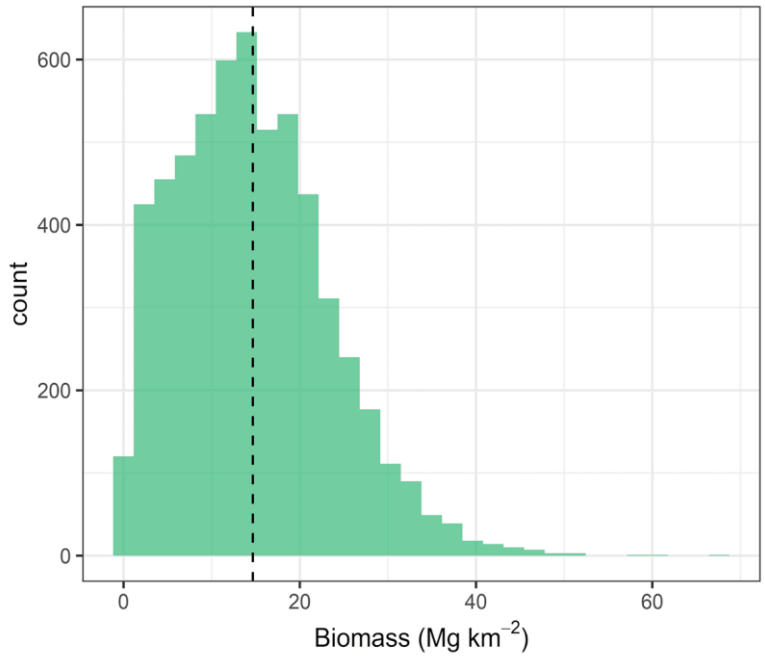

Figure S3.2.2. Above ground biomass of *J. thurifera* estimated from top of canopy height and canopy fraction at a resolution of 26.9 m for areas known to be dominated by *J. thurifera.*

S3.3. Landscape above ground biomass model - alternative forms

We present the results of alternative models of above ground biomass ($Mg.ha^{-1}$) as a function of variables derived from a structure from motion canopy height model, along with associated root mean squared errors, mean absolute errors, percentage biases, and anti-logarithmic correction factors (Table S3.3.1). Biomass was modelled using a leave one out regression as a function of mean top of canopy height (*TCH*), cover fraction at 0.5 m (*CF*) and a compound variable of *TCH* and *CF* (*TCH* X *CF*, see main text). Coefficients for the final model are presented in the main text, and coefficients of the alternate models are given here in equations Eq. S3.3.1 and Eq. S3.3.2.

$$Biomass_{CF} = C_{CF}(27.73 \times CF^{0.75}) \quad \text{(Eq. S3.3.1)}$$

$$Biomass_{TCH} = C_{TCH}(2.01 \times TCH^{2.48}) \quad \text{(Eq. S3.3.2)}$$

Table S3.3.1. Root mean squared errors (RMSE), mean absolute errors (MAE), percentage biases (Bias), and anti-logarithmic correction factors (C_i) for each model structure used to model above ground biomass.

Explanatory Variable	RMSE	MAE	Bias (%)	C_i
TCH	0.904	0.761	39.7	1.50
CF	0.397	0.335	15.9	1.08
TCH X CF	0.456	0.358	10.4	1.11

References

Baskerville, G. L. 1972. "Use of Logarithmic Regression in the Estimation of Plant Biomass. Canadian Journal of Forest Research 2: 49–53. https://doi.org/10.1139/x72-009

Natural Environmental Research Council (NERC) Geophysical Equipment Facility. n.d. "Geophysical Equipment facility." Equipment service. Accessed at http://www.gef.nerc.ac.uk

Supporting information to the paper

Bentley L., A. Forner, S. Khoury, F. Valladares, D.A. Coomes, and I. Martín-Forés. Turning Mediterranean farmlands into priority habitats: Natural expansion of juniper woodlands after agricultural abandonment. *Journal of Vegetation Science*.

Appendix S4. Juniper growth at the individual scale and effects of sex and intraspecific competition.

The Hegyi index is the most classical spatial competition index which allows quantitative calculation of the effect of intraspecific competition (Uhl et al. 2015). This index considers the distance between the target tree and its competitors at a given distance, and their relative size to the target tree. It can be calculated following Eq. S4.1.

$$DCI_j = \sum_{i=1}^{n} \left(\frac{d_i}{d_j} \cdot \frac{1}{1 + DIST_{ij}}\right) \quad \text{(Eq. S4.1)}$$

where j is the target tree, i its neighbour, d_j and d_i their diameters respectively, and $DIST_{ij}$ represents the distance between both trees.

To determine whether the lack of a significant effect of sex on variation in individual above ground biomass ($Biomass_{Tree}$) was due to the allometric equations used not being sex dependent, we repeated the analysis, using variation in tree height and basal area as our response variables, rather than above ground biomass. When calculating Hegyi coefficients, a threshold of 10 m was used for the analysis of tree height and a threshold of 20 m was used for basal area, which was analysed as a natural logarithm of basal area. The assumptions of normality were met for all regression analyses.

Both tree height (*TH*) and basal area (*BA*) were also found to vary significantly with tree age (*TH* Wald interval: 2.5 % = 0.048, 97.5 % = 0.075; *BA* Wald interval: 2.5 % = 0.035, 97.5 % = 0.055) and Hegyi competition coefficients (*TH* Wald interval: 2.5 % = -0.320, 97.5 % = -0.163; *BA* Wald interval: 2.5 % = -0.337, 97.5 % = -0.227), and in both cases, sex was removed from the model based on model AIC (Table S4.1). Plot identity explained 16.3 % and 34.5 % of the variance in tree height and basal area, respectively. Coefficient estimates for both models are shown in equations (Eq. S4.2 – Eq. S4.3). AIC scores associated with all three model structures are provided in Table S4.1. Starting fixed effect model structures are shown in equations (Eq. S4.2 – Eq. S4.6).

$$TH = 3.346 + 0.062\, Age - 0.241\, H_{10} \quad \text{(Eq. S4.2)}$$

$$\ln(BA) = -5.164 + 0.045\, Age - 0.282\, H_{20} \quad \text{(Eq. S4.3)}$$

$$\ln(Biomass_{Tree}) = a + b\, Age + c\, H_{20} + d\, Sex \quad \text{(Eq. S4.4)}$$

$$TH = a + b\, Age + c\, H_{10} + d\, Sex \quad \text{(Eq. S4.5)}$$

$$\ln(BA) = a + b\, Age + c\, H_{20} + d\, Sex \quad \text{(Eq. S4.6)}$$

Table S4.1. Model selection for equations (S4.4-S4.6) explaining variation in the natural logarithm of above ground biomass (*ln(*$Biomass_{Tree}$*)*), tree height (*TH*) and the natural logarithm of basal area (*ln(BA)*). Where '.' refers to the starting model structure shown in equations (Eq. S4.4–Eq. S4.6) and H_{10} and H_{20} to the Hegyi coefficient using a threshold of 10 m or 20 m respectively.

Model structure	AIC	Model structure	AIC	Model structure	AIC
ln($Biomass_{Tree}$) ~ .	390.7	TH ~ .	537.1	ln(BA) ~ .	422.6
ln($Biomass_{Tree}$) ~ . - Sex	384.7	TH ~ . - Sex	533.0	ln(BA) ~ . - Sex	417.5
ln($Biomass_{Tree}$) ~ . - H_{20}	447.0	TH ~ . - H_{20}	552.5	ln(BA) ~ . - H_{20}	480.0
ln($Biomass_{Tree}$) ~ . - Age	458.5	TH ~ . - Age	597.7	ln(BA) ~ . - Age	476.1
ln($Biomass_{Tree}$) ~ . - Sex - Age	455.9	TH ~ . - Sex - Age	596.5	ln(BA) ~ . - Sex - Age	475.2
ln($Biomass_{Tree}$) ~ . - H_{20} - Age	511.3	TH ~ . - H_{10} - Age	619.7	ln(BA) ~ . - H_{20} - Age	536.2
ln($Biomass_{Tree}$) ~ . - H_{20} - Sex	442.1	TH ~ . - H_{10} - Sex	548.7	ln(BA) ~ . - H_{20} - Sex	475.6
ln($Biomass_{Tree}$) ~ 1	511.5	TH ~ 1	619.5	ln(BA) ~ 1	536.8

References

Uhl, E., P. Biber, M. Ulbricht, et al. 2015. "Analysing the effect of stand density and site conditions on structure and growth of oak species using Nelder trials along an environmental gradient: experimental design, evaluation methods, and results." Forest Ecosystems 2: 17. https://doi.org/10.1186/s40663-015-0041-8

Supporting information to the paper

Bentley L., A. Forner, S. Khoury, F. Valladares, D.A. Coomes, and I. Martín-Forés. Turning Mediterranean farmlands into priority habitats: Natural expansion of juniper woodlands after agricultural abandonment. *Journal of Vegetation Science*.

Appendix S5. Effect of topography and interspecific competition on juniper growth at the landscape scale.

We investigated the effects of local topography on juniper growth rates at the landscape scale to assess environmental suitability. The analysis was carried out on 1,500 randomly selected pixels within the region of known juniper woodland. Solar insolation was calculated as previously described. Values for elevation, slope and solar insolation previously obtained were scaled and centred prior to analysis. Correlations between continuous explanatory variables were assessed prior to analysis using Kendall's rank correlation (Table S5.1). Insolation was closely correlated with aspect but not elevation or slope (Table S5.1).

Table S5.1 Kendall's rank correlation coefficient for woodland age, elevation, slope and solar insolation in the 1500 points used in the analysis of above ground biomass (see main text).

	Age	**Elevation**	**Slope**	**Insolation**
Age	-	-	-	-
Elevation	-0.042	-	-	-
Slope	0.048	0.019	-	-
Insolation	-0.014	-0.049	-0.022	-

We manually classified dwarf shrubland cover within 30 m pixels of juniper woodland as low, medium and high-density shrub cover using the photogrammetry derived orthomosaic (Figure S5.1).

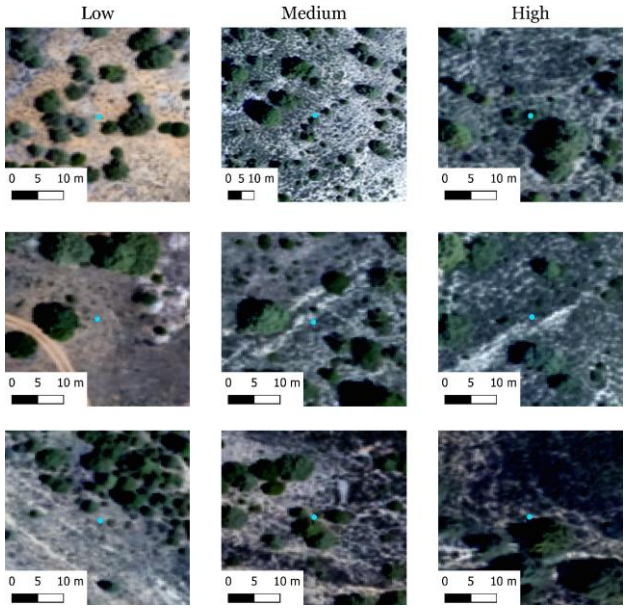

Figure S5.1. Reference examples of dwarf-shrub cover within 30 m pixels of juniper woodland, manually classified as low, medium and high-density shrub cover.

Associations between the distribution of dwarf shrub cover and both age and topographically derived variables were ruled out using an ordination (Figure S5.2).

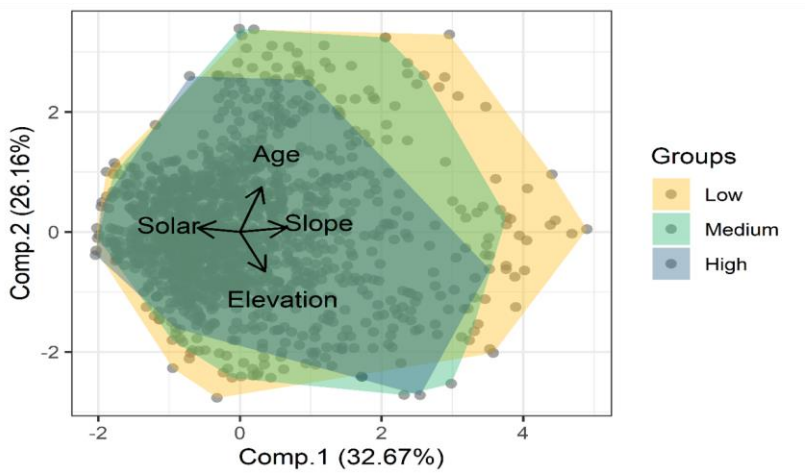

Figure S5.2. Ordination of woodland age, slope, elevation, and solar insolation in the dataset used to analyse variation in above ground biomass, showing the first two axes of a principal component analysis. Hulls for each class of shrubland density are shown.

Model coefficient estimates of the effects of topography and interspecific competition on juniper growth at the landscape scale are provided in Table S5.2.

Table S5.2. Effect sizes and significance of time since colonisation (age), topography and interspecific competition (dwarf- shrubland cover) on *J. thurifera* growth at the landscape scale, estimated via a spatial simultaneous autoregressive error model using a square-root transformation of the response variable.

	Estimate	**Standard Error**	**Z value**	***P* value**
Intercept (Low dwarf-shrubland cover)	3.273	0.074	44.3	< 0.0001
Age	0.040	0.002	16.0	< 0.0001
Elevation (scaled)	-0.305	0.012	-25.3	< 0.0001
Insolation (scaled)	-0.233	0.105	-2.2	0.0266
Medium dwarf-shrubland cover	-0.358	0.047	-7.6	< 0.0001
High dwarf-shrubland cover	-0.601	0.068	-8.9	< 0.0001
Age x Insolation (scaled)	0.015	0.004	4.0	< 0.0001